

Persistent Room-Temperature Phosphorescence from Purely Organic Molecules and Multi-Component Systems

Zhu Wu, Jörn Nitsch, and Todd B. Marder*

Recently, luminophores showing efficient room-temperature phosphorescence (RTP) have gained tremendous interest due to their numerous applications. However, most phosphors are derived from transition metal complexes because of their intrinsic fast intersystem crossing (ISC) induced by strong spin-orbit coupling (SOC) constants of the heavy metal. Metal-free RTP materials are rare and have become a promising field because they are inexpensive and environmentally friendly. This review summarizes organic molecular materials with long triplet lifetimes at room temperature from the perspective of whether they stem from a molecular or multi-component system. Among purely organic phosphors, heteroatoms are usually introduced into the backbone in order to boost the singlet-triplet ISC rate constant. In multi-component systems, useful strategies such as host-guest, polymer matrix, copolymerization, and supramolecular assembly provide a rigid matrix to restrict nonradiative pathways thus realizing ultralong RTP.


1. Introduction

Persistent room-temperature phosphorescent (RTP) luminophores have gained remarkable interest recently for a number of applications in security printing,^[1] organic light-emitting diodes (OLEDs),^[2] optical storage,^[3] time-gated biological imaging,^[4] and oxygen sensors^[5] due to their unique long emission lifetimes, excellent signal-to-noise ratio, large Stokes shifts, and simple operation. At present, the majority of persistent RTP materials are heavy metal-containing complexes, in which charge transfer between metal and ligand mixes singlet and triplet excitons and strong spin-orbit coupling (SOC) improves the rate of intersystem crossing (ISC), and enhances the rate of phosphorescence decay.^[6] However, many metal-based phosphors are toxic, high in cost, and difficult to process compared to organic RTP materials which are environmentally friendly, inexpensive, and convenient to prepare.^[7] Thus, the

demand to develop novel purely organic RTP materials has grown recently. Unlike transition metal-containing phosphors, organic materials with persistent luminescent phosphorescence emission are still limited because both the radiative pathway from T_1 to S_0 is spin forbidden and the ISC rate from excited singlet to triplet states is relatively slow.^[8] The major challenge is to suppress nonradiative pathways from T_n , which are usually fast processes. Therefore, specific strategies are designed to enhance the quantum yield and lifetime of RTP by promoting the rate of ISC and, at the same time, restricting the non-radiative relaxation of the triplet states,^[9] including incorporating heavy atoms,^[10] introducing carbonyl groups bearing lone pairs,^[11] polymerization methods,^[12] constructing a supramolecular framework based on self-assembly properties,^[13] utilizing host-guest systems,^[14] or carbon dots (CDs).^[15] Although many approaches have been developed to populate triplet excitons by enhancing SOC, which can be achieved by taking full advantage of El-Sayed's rule,^[16] organic phosphors are still limited to certain categories of compounds, such as phenazine,^[17] phenothiazine,^[18] naphthylamide,^[19] and boronic acid^[20] and boronic ester^[21] derivatives. More recently, our group reported the first triarylborane compounds without lone pairs which exhibit persistent RTP.^[22] Bechtold et al. also reported a phosphorescent arene in which the non-planar configuration leads to enhanced SOC and a high energy of the T_1 state with a quantum yield up to 5.6%.^[23] All of these findings greatly expand the types of organic RTP materials. Moreover, they give useful guidance to understand the relationships between structure and property.^[24]

It is important to note that for RTP, which has in many cases an intrinsic low photoluminescence quantum yield, special attention must be paid to how the measurements are performed and to the purity of the sample under examination since the smallest impurity can lead to a completely wrong or at least misleading conclusion.^[4] Phosphors derived from carbazole and related functional groups should be re-examined carefully with respect to possible impurities, as pointed out recently by Liu et al.^[25] At the same time, it should be noted that confirmed, pure carbazole-based molecules do exhibit persistent phosphorescence at room temperature.^[26] Carbazole-based phosphors are indeed interesting and still promising, but require extremely careful study.^[27-43] Very recently, Babu et al. introduced a number of typical carbazole-based phosphors in their review.^[44] Therefore, in our review, we present

Z. Wu, Dr. J. Nitsch, Prof. T. B. Marder
Institut für Anorganische Chemie and Institute for Sustainable
Chemistry & Catalysis with Boron
Julius-Maximilians-Universität Würzburg
Am Hubland, 97074 Würzburg, Germany
E-mail: todd.marder@uni-wuerzburg.de

 The ORCID identification number(s) for the author(s) of this article can be found under <https://doi.org/10.1002/adom.202100411>.

© 2021 The Authors. Advanced Optical Materials published by Wiley-VCH GmbH. This is an open access article under the terms of the Creative Commons Attribution License, which permits use, distribution and reproduction in any medium, provided the original work is properly cited.

DOI: 10.1002/adom.202100411

some additional carbazole-based phosphors in Section 3.6. Most published reviews do not clearly indicate the significance of impurity effects, and may lead to misunderstandings about RTP research.^[45] Indeed, we note that extra care needs to be taken to avoid the possibility that RTP phenomena result from trace impurities, as the problem may extend well beyond the carbazole systems. In our review, we present the results and explanations offered by the original authors. We hope that this encourages others to explore the field, and perhaps to re-examine some of the previously reported examples.

This review is structured as follows. In Section 2, the photo-physical parameters (Φ_{isc} , Φ_p , τ_p) required for RTP are presented.^[46] In Section 3, purely organic room-temperature phosphors are classified according to their categories of functional groups which include amide derivatives, boron- and sulfur-containing compounds, quinoxaline derivatives, siloxy group-induced, and carbazole-based phosphors. In the last part of Section 3, several nonclassical RTP materials are also introduced. Section 4 provides a summary of multi-component RTP systems, and popular, current strategies to construct multi-component RTP materials, host-guest systems, and supramolecular systems. As it is hard to distinguish whether carbon dots (CDs) are purely organic or multicomponent systems in some cases, we introduce them in Section 5. In the last two sections, we give our future perspectives and conclusion.

2. Physical Parameters of RTP

As described in **Figure 1**, electrons of organic RTP molecules are excited from the S_0 state to S_1 – S_n states. The excited singlet state can fluoresce and also undergo nonradiative decay to the ground state or relax to a triplet state through an ISC process when the SOC is strong enough and when the energy gap ΔE_{ST} between the states is sufficiently small enough. According to Kasha's rule,^[47] if the populated triplet excited state T_n is a higher-lying state, it decays quickly to T_1 through internal conversion (IC). Triplet to singlet ground state transitions through radiative decay lead to phosphorescence which is often a slow process (ms) compared to the lifetime of fluorescence (ns), due to the forbidden nature of transitions from T_1 to S_0 . This is also the reason that our naked eye can observe the afterglow of phosphorescence. The rate of nonradiative decay is often higher

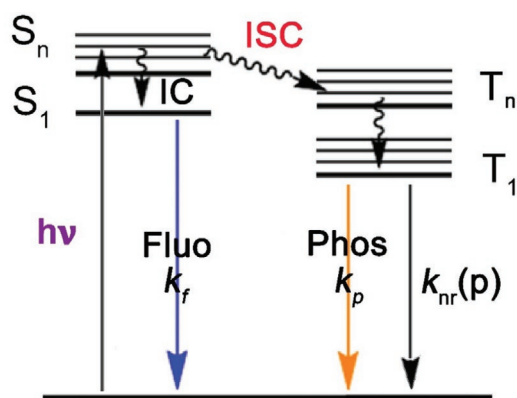


Figure 1. Jablonski diagram.

than the radiative decay rate from T_1 to S_0 at room temperature. Besides oxygen and moisture quenchers, molecular motion (rotations and vibrations) play an important role in nonradiative decay processes. Therefore, phosphorescence from pure organic molecules is typically observed under an inert atmosphere and at low temperature. Approaches such as imbedding the emitter into a rigid matrix or crystallization are used to restrict molecular motions to restrict nonradiative decay for achieving long-lived RTP according to Equation (1):^[48]

$$\tau_p = 1/(k_p + k_{nr} + k_q) \quad (1)$$

where τ_p is the phosphorescence lifetime, k_p is the radiative decay rate, and k_{nr} is the non-radiative decay rate from T_1 to S_0 , and k_q is the quenching rate of the triplet excited state by quenching species. In addition, in organic systems, ISC is often not efficient, but can be accelerated by SOC utilizing heavy atoms (Br, I) or by $n-\pi^*$ transitions by introducing elements bearing lone pairs (N, O, S). Based on El-Sayed's rule,^[16] the ISC rate constant will be enhanced when the two electronic transition states involved belong to different orbital types (${}^1n\pi^* \rightarrow {}^3\pi\pi^*$ or ${}^1\pi\pi^* \rightarrow {}^3n\pi^*$), leading to an increased phosphorescence quantum yield according to Equations (2) and (3):^[47]

$$\phi_{isc} = k_{isc} / (k_f + k_{ic} + k_{isc}) \quad (2)$$

$$\phi_p = \phi_{isc} k_p / (k_p + k_{nr} + k_q) \quad (3)$$

where k_f is the fluorescence decay rate from S_1 to S_0 state, k_{ic} is the IC rate from S_1 to S_0 , k_{isc} is the ISC rate from S_1 to T_1 , and Φ_{isc} is the ISC quantum yield from S_1 to T_1 . In some cases, the triplet state in purely organic materials can be stabilized by intermolecular interactions even under ambient conditions, while triplet-triplet annihilation (TTA) is effectively suppressed, resulting in persistent RTP.^[49]

3. Single Component RTP Systems

3.1. Amide Derivative-Based RTP Systems

To develop metal-free RTP materials, heteroatoms are commonly used elements as they provide lone pairs which speed up the ISC process. In addition, hydrogen bond interactions also suppress nonradiative decay. Amides and their derivatives are good candidates for the construction of RTP materials. In 2018, Shi et al. reported ImBr (**Figure 2a**) with a dual emission, emitting white-light due to the mixture of blue fluorescence and yellow phosphorescence.^[50] Persistent RTP from ImBr is likely induced by the bromine atom which introduces strong SOC. In addition, non-centrosymmetric packing and hydrogen bonds, immobilizing the molecular conformations in the crystalline state, reduce nonradiative decay channels (**Figure 2c**). In 2009, Sukumaran et al. first reported a solvent-free liquid long alkyl chain-substituted bromonaphthalimide **2** (**Figure 2d**) which exhibits RTP in air.^[51] Compound **1** shows phosphorescence lifetimes of 6.2 ms at 25 °C and 319 ms at –196 °C while compound **2** exhibits phosphorescence lifetimes

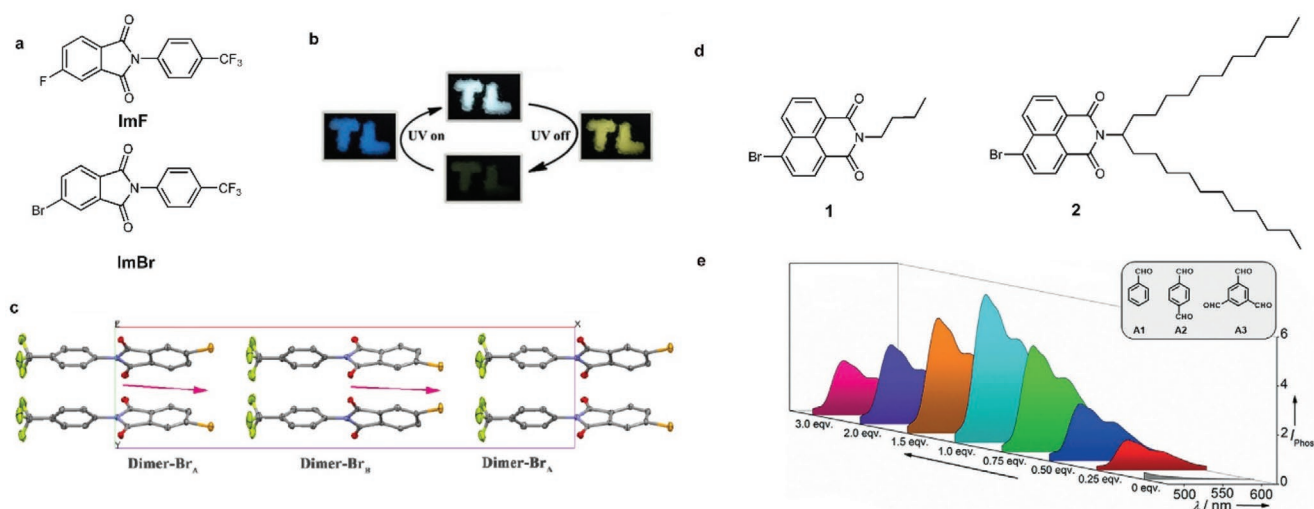


Figure 2. a) Molecular structures of ImF and ImBr. b) Tricolor emission switching of ImBr. Reproduced with permission.^[50] Copyright 2018, Wiley-VCH. c) Crystal packing mode of ImBr. d) Molecular structures of compounds 1 and 2. e) Phosphorescence spectral changes of 2 with increasing equivalents of A2 at RT in air. Reproduced with permission.^[51] Copyright 2019, Wiley-VCH.

of 5.7 ms at 25 °C and 210 ms at 196 °C. The solvent-free liquid 2 shows phosphorescence emission at 594 nm at 25 °C in air. According to calculations, a small ΔE_{ST} facilitates ISC, leading to RTP from compound 2. Interestingly, these phosphors can be used as a sensor of carbonyl compounds. The intensity of phosphorescence from 2 is gradually enhanced with increasing amounts of carbonyl up to 1.0 equivalent (Figure 2e). The authors proposed that halogen-bonding in the supramolecular system assists in-plane intermolecular interactions which promote SOC to generate triplet states efficiently. In the same year, Ma et al. designed several purely organic polymers (PVP-BrHexene, PNVL-BrNpA, PVP-BrNpA, PVP-BA, PNVL-BrHexene, and PNVL-BA) based on lactams (Figure 3a,b).^[52] Except for PNVL-BrHexene, the phosphorescence lifetimes (τ_p) of the polymers vary from 0.13 to 0.94 ms, with phosphorescence quantum yields (Φ_p) ranging from 0.4% to 1.6%. Lactam groups bearing lone pairs not only provide hydrogen bonds but also enhance the ISC rate. Furthermore, the polymer matrix provides a rigid environment which restricts molecular motions, resulting in efficient RTP.

In 2020, Bo et al. reported two groups of ladder-type organic phosphors (Figure 4a).^[53] In group B, they utilized the bulky norbornyl (NB) moiety to separate *N*-methyl phthalimide groups, achieving persistent RTP for which the phosphorescence lifetime can reach 357.1 ms with quantum yields up to a relatively high value of 2% (Figure 4a). By analyzing the crystal structure, they found that a parallel stacking alignment reduces the π - π distances which generate stronger hydrogen to oxygen and π interactions between molecules (Figure 4b). This also facilitates the S_1 to T_n transition, thus increasing the phosphorescence efficiency. They also demonstrated an application in the field of dual data encryption which is based on the reversible photochromic properties of α -PA (Figure 4c,d). In the solid-state, α -PA shows no color change under short irradiation times by UV light (254 nm). In contrast, upon irradiation for up to 10 s, the color of the sample changes from achromaticity to yellow. In addition, the blue emission of the sample is quenched. After irradiation with daylight or heating, the sample becomes colorless again.

3.2. Boron-Containing RTP Materials

3.2.1. Boronic Acid and Ester Phosphors

Boron-containing RTP luminophores have gained considerable interest because of their easy accessibility, low cost, and simple modification. In addition, oxygen atoms in boronic acids and esters can promote ISC and hydroxy groups in boronic acids can form strong hydrogen bonds. In 2017, Yuasa et al. reported

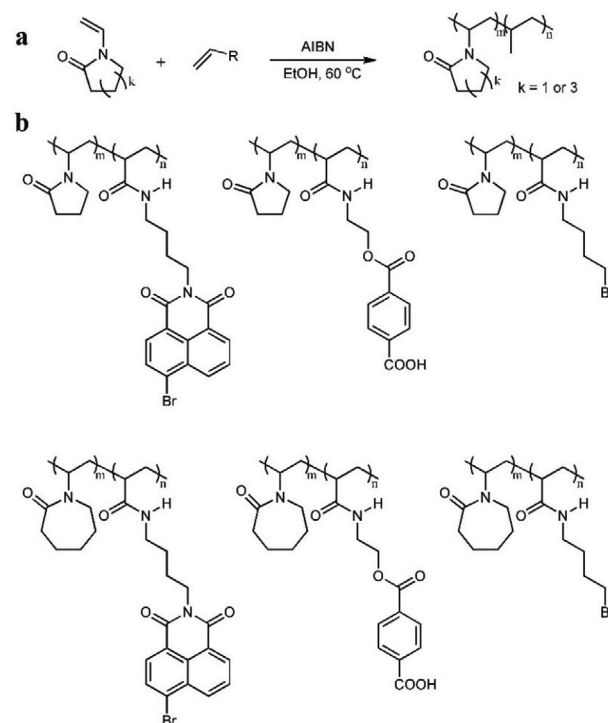


Figure 3. a) Method for polymerization. b) Structures of the PVP- and PNVL-polymers. Reproduced with permission.^[52] Copyright 2019, Wiley-VCH.

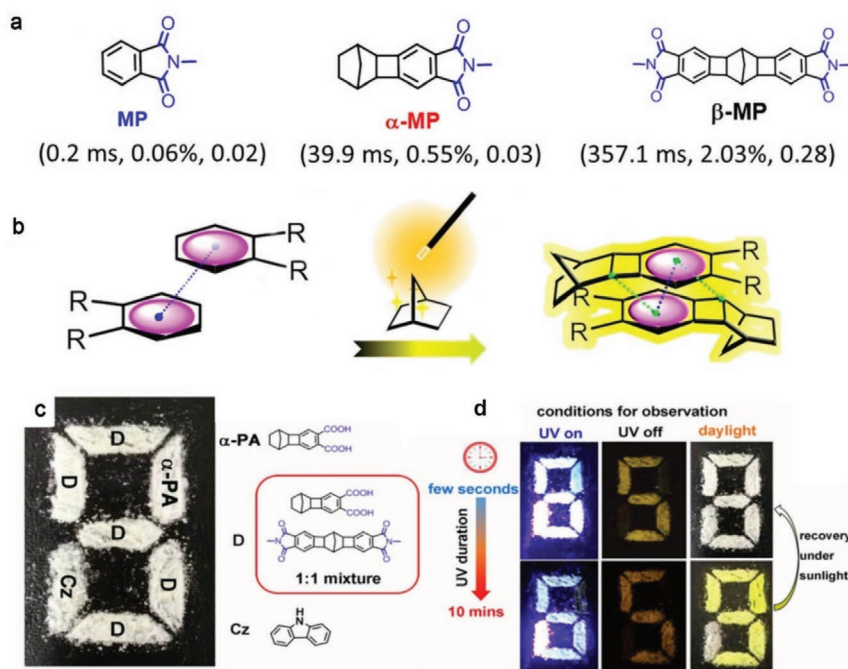


Figure 4. a) Molecular structure of the luminophores in the crystalline powder state. b) The vital role NB plays in triggering RTP. c) The different parts of the pattern “8”; d) pictures of the pattern “8” taken after different UV exposure times. Reproduced with permission.^[53] Copyright 2020, Wiley-VCH.

the crystalline phenylboronic acid derivatives PB, PDB, and PDBEG (Figure 5a) in which the phosphorescence lifetime of PDBEG reaches 1.6 s.^[20] According to the photophysical data obtained in the crystal matrix, they suggested that charge-transfer complexes formed between two neighboring molecules play a major role in persistent RTP. In this complex, ISC is driven by hyperfine-coupling, which is termed HFC-driven. This new phosphorescence mechanism through CT formation provides useful design guidance for new types of photosensitizers. Meanwhile, Li's group designed and synthesized an AIEgen DPPBO (Figure 5b; AIE = aggregation-induced emission) stimulated by mechanical forces with dual fluorescence and phosphorescence.^[21] Based on analysis of the crystal structure, combined with theoretical studies, they proposed that the polar boron oxygen bond of the ester contributes with the oxygen lone pairs to produce strong intermolecular and intramolecular interactions (Figure 5c), but also to the population of triplet states by promoting the spin-forbidden transition of excited states from singlet to triplet via ISC. Li's group also reported that the commercially available PBA-MeO (4-methoxyphenyl)boronic acid (Figure 5d) exhibits persistent green RTP for which the phosphorescence lifetime can reach 2.24 s.^[54] Their findings suggest that the rigidification and interactions between neighboring molecules in the aggregated state prohibit rapid nonradiative decay. Moreover, the triplet states are stabilized by effective π - π stacking which enhances the ISC process. It is one of the longest lifetimes for an organic molecule with a single component reported so far. In 2019, Su et al. thoroughly investigated the RTP properties of boronic ester-substituted phenoxathiine-based derivatives i-PXT-BPin,

PXT-BPin, and TE-BPin (Figure 5e).^[55] However, it is noted that the efficiency of RTP was not always enhanced in the boronic esters examined. Only PXT-BPin was found to have a high phosphorescence quantum yield ($\Phi_p = 20\%$). By analysis of the crystal structure, they found that PXT-BPin adopts a more condensed intermolecular packing mode compared to other molecules in the crystalline state and has an (n, π^*) transition, which accelerates the ISC process (Figure 5f). Moreover, the molecular vibrations and rotations were significantly reduced in crystalline PXT-BPin, resulting in the preservation of a high quantum yield. Fukushima's group investigated 19 arylboron compounds and measured their photophysical properties (Figure 6a,b). These compounds displayed lifetimes of up to several seconds at room temperature in air.^[56] Theoretical calculations for boronic ester 2 (Figure 6a) indicate that the (pinacol)B-C_{ipso} moiety has an out-of-plane distortion in the T₁ state, which may mix σ and π orbitals to accelerate ISC. However, it is not clear how the structural changes influence the RTP in the solid-state. They proposed that solid-state molecular packing may have an important effect on the phosphorescence properties, compared to the positions and numbers of boron substituents on the phenyl ring. This exciting finding inspired researchers to use boronic acid and ester moieties to develop new RTP phosphors. Liang's group developed a highly sensitive oxygen detector (TBBU) embedded in PMMA films (Figure 6c). The value of Φ_p is as high as 13% and the lifetime is as long as 350 ms under vacuum.^[57] TBBU is designed as a non-coplanar D- π -A structure without symmetry which uses the boronic ester as the acceptor. It allows intermolecular aromatic rings to adopt a side-by-side packing mode with a head-to-tail arrangement

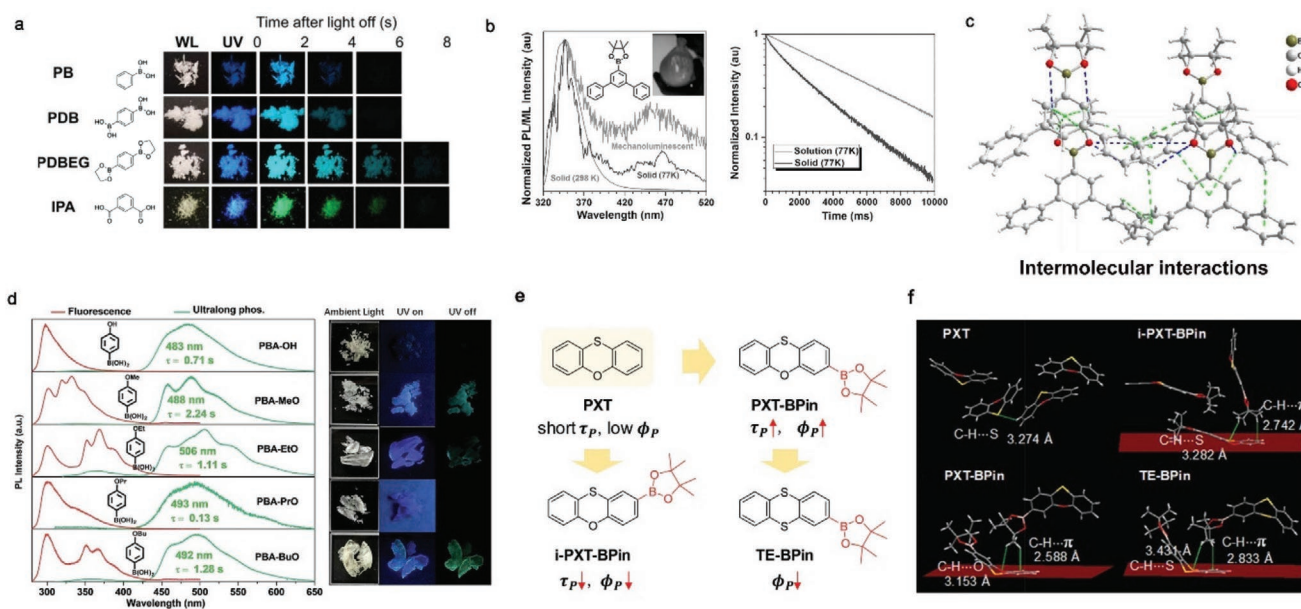


Figure 5. a) Chemical structures and afterglow images of PB, PDB, PDBEG, and IPA. Reproduced with permission.^[20] Copyright 2017, Wiley-VCH. b) Photoluminescent and mechanoluminescent spectra of DPP-BO at 298 and 77 K in the solid-state. c) The intermolecular C—H \cdots π interactions are displayed in green lines and the C—H \cdots O interactions are displayed in blue lines. b,c) Reproduced with permission.^[21] Copyright 2017, Wiley-VCH. d) PL spectra of the crystalline PBA, and the corresponding RTP photographs taken before and after UV light irradiation. Reproduced with permission.^[54] Copyright 2017, The Royal Society of Chemistry. e) Chemical structures of PXT, i-PXT-BPin, PXT-BPin, and TE-BPin. f) Single-crystal structures and intermolecular interactions of PXT, PXT-BPin, i-PXT-BPin, and TE-BPin. e,f) Reproduced with permission.^[55] Copyright 2019, The Royal Society of Chemistry.

(Figure 6d). Therefore, the large pores retained in the solid-state increase the sensitivity for oxygen detection. On the one hand, with the addition of O₂, the color of the doped film turns deep blue from pink-blue and enables a visual detection of oxygen (Figure 6e). On the other hand, the value of 1/ τ_p is positively correlated with the O₂ concentration value, which enables the quantitative detection of oxygen. This method demonstrates a simple and reliable way to detect oxygen by using persistent RTP properties.

3.2.2. Triarylborane Phosphors

Compared to boronic acids and esters, triarylborane-based phosphors are easier to modify because of possible substitution at the three phenyl rings.^[58,59] In addition, increased π to empty boron p orbital transitions may also accelerate the rate of the ISC process. In 2020, Zhao's group reported a triarylborane-based biphenyl phosphor derivative (Br₂-BN-BPh) (Figure 7a).^[60] The highly twisted biphenyl skeleton separates the HOMO and LUMO, leading to a small value of ΔE_{ST} (Figure 7b). Both the small ΔE_{ST} and the bromine heavy atoms can improve the SOC and thus increase the ISC rate. In addition, the rigid backbone of Br₂-BN-BPh and the boron to nitrogen and π - π interactions within molecules can suppress nonradiative decay, resulting in a phosphorescence quantum yield as high as 36%. In the same year, our group designed triarylboranes 1–4 (Figure 7c) with different numbers of —CH₃ moieties on the benzene ring.^[22] Interestingly, crystalline **3** (tris(2,6-dimethylphenyl)

borane) exhibits long-lived yellow phosphorescence with a lifetime of 0.5 s. Compounds **1** and **3** are the first triarylborane-based phosphors without any lone pairs or heavy atoms which display ultralong RTP under ambient conditions. Theoretical calculations reveal that transitions between (σ , B p) and (π , B p) can also speed up the rate of ISC (k_{isc}), which is an addition to the normal ISC process, and which is accelerated by transitions between ¹(n, π^*) and ³(π , π^*) (Figure 7d). Moreover, compound **3** has the highest phosphorescence efficiency among the four compounds. By analysis of the crystal structure, we found that there is a void in the unit cell of **3**. It is proposed that the presence of the voids may play an important role, for example enhancing π - π interactions between these aryl rings when excited, which may help to suppress nonradiative decay and achieve persistent RTP.

3.2.3. Four-Coordinate Boron Phosphors

In 2007, Fraser's group reported a single-component, multi-emissive (RTP, delayed fluorescence and fluorescence) difluoride dibenzoylmethane coupled with poly(lactic acid).^[61] This multifunctional material is responsive to many factors such as temperature and oxygen (Figure 8a). Two years later, they developed a difluoroboron dibenzoylmethane-poly(lactic acid) BF₂dbm(I)PLA substituted by iodine.^[62] By controlling the PLA chain length by lactide polymerization, this purely organic phosphor can be used for versatile applications. On the one hand, a low-molecular-weight P1 film with a dominant

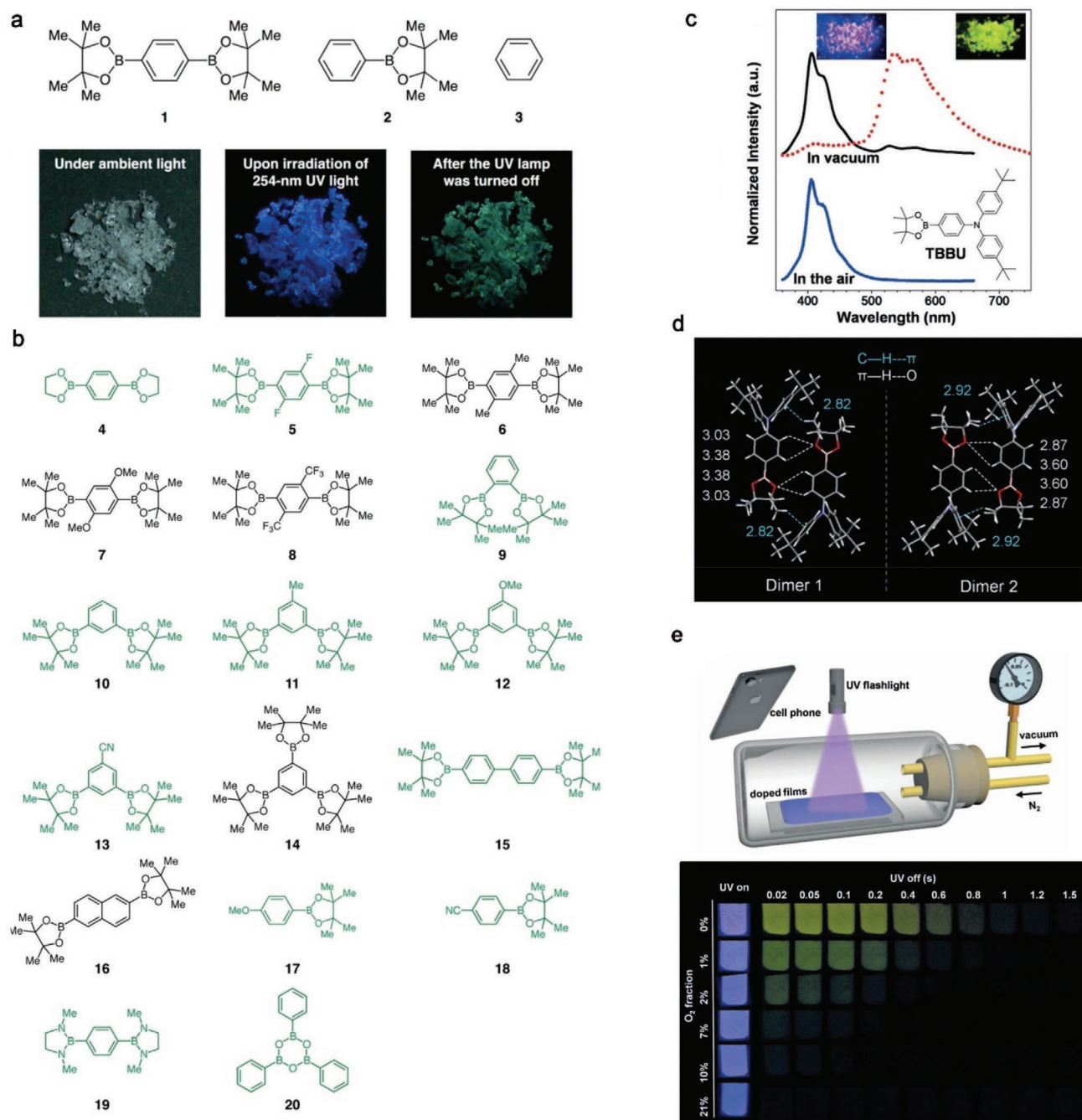


Figure 6. a) Molecular structures of 1–3. Afterglow photographs of crystalline 1. b) Molecular structures of boron compounds in which compounds with RTP are shown in green and the other are in black. Reproduced with permission.^[56] Copyright 2017, American Chemical Society. c) PL spectra of crystalline TBBU. Inset: digital images at room temperature. d) Crystal structure of TBBU. e) Oxygen detection with the TBBU doped film (top) and persistent RTP images (bottom) of the doped film at different oxygen concentrations. Reproduced with permission.^[57] Copyright 2019, Wiley-VCH.

phosphorescence and weak fluorescence is a promising ratiometric oxygen sensor. On the other hand, higher molecular weight polymer boron nanoparticles (NPs) P2 with balanced fluorescence and phosphorescence emission can serve as ratiometric tumor hypoxia imaging agents (Figure 8b). In 2007, Fu et al. developed an organic phosphorescence nanowire laser (Figure 8c) using a difluoroboron compound substituted

by sulfur.^[63] The lone pairs of the nitro group and the sulfur substituent induced an intramolecular charge transfer (ICT) transition leading to highly efficient ISC from S_1 (n, π^*) to T_1 (π, π^*) ($\Phi_{ISC} = 100\%$) which enables organic solid-state laser phosphorescence with an emission peak at 650 nm. This work successfully applied a four-coordinate boron RTP material in practical use as a laser.

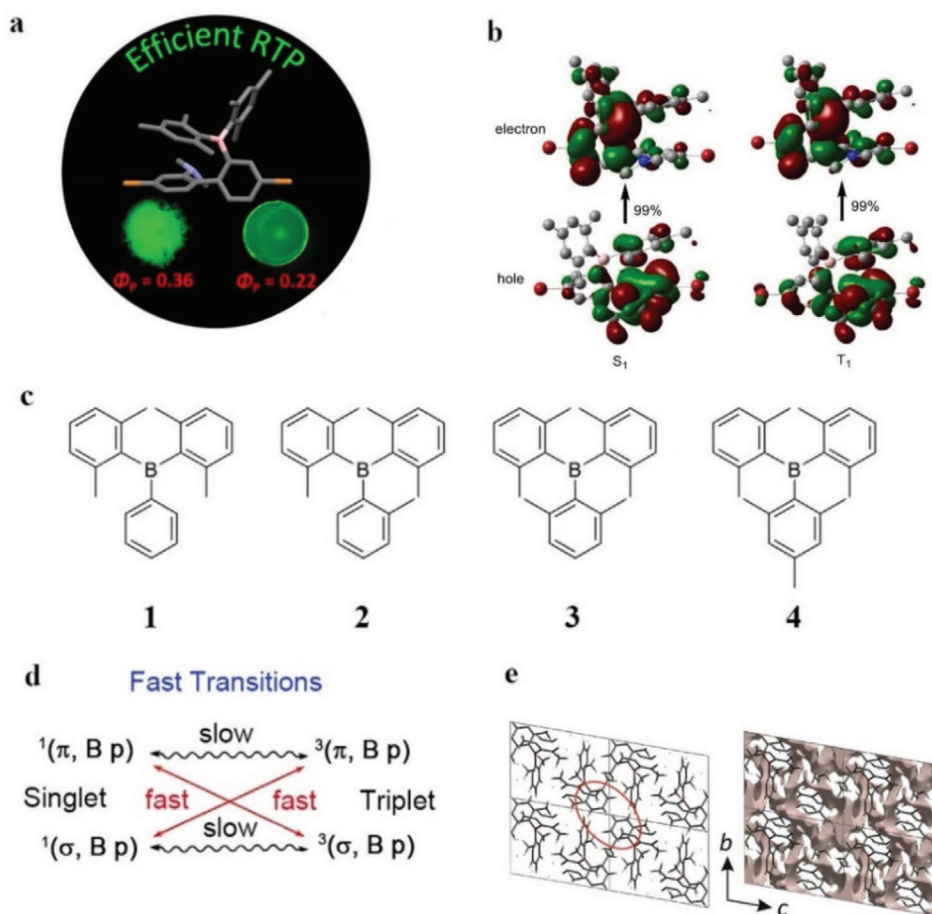


Figure 7. a) Chemical structure of Br₂-BN-BPh. b) Natural transition orbitals for the S₁ and T₁ states of Br₂-BN-BPh. Reproduced with permission.^[60] Copyright 2020, American Chemical Society. c) Molecular structures of compounds 1–4. d) Fast transitions between (σ, B p) and (π, B p) and (σ, B p) and (σ, B p). e) Crystal structure of compound 3, and plot of the Hirshfeld surface of the crystal voids (0.002 a.u.). Reproduced with permission.^[22] Copyright 2020, Wiley-VCH.

3.3. Sulfur-Containing RTP Materials

3.3.1. Benzothiophene Derivative-Based Phosphors

Sulfur is one of the most important elements used in RTP materials. First, the lone pairs of sulfur provide n to π transitions and thus increase ISC according to El-Sayed's rule. Moreover, multiple intermolecular interactions between S⋯H or S⋯π can suppress nonradiative pathways by restricting molecular rotations and vibrations. In 2020, Wolf et al. reported diarylethene luminophores **1o**, **2o**, and **3** containing quinoline moieties (Figure 9a).^[64] Compound **1o** shows typical diarylethene photocyclization character in CH₂Cl₂ solution when irradiated by 365 nm UV, with its color turning from colorless in the open form to red in the closed form. Phosphor **3** is achieved by methylation of the quinoline nitrogen of **1o**. The emission peak at 575 nm showed a phosphorescence lifetime as long as 1.9 ms at room temperature while the higher energy peak at 540 nm exhibited a much longer lifetime of up to 244 ms at 77 K (Figure 9b,c). Theoretical studies revealed that the HOMO and LUMO are separated to a large extent in the space, which

can promote ISC (Figure 9d). In addition, charge transfer from the benzothiophene to the quinolinium group may also enhance ISC. Moreover, strong interactions between the DAE (diarylethene) cation and the [BF₄]⁻ anion prevent amorphous **3** from coming into contact with triplet quenching species and inhibit vibrational relaxation.

3.3.2. Phenothiazine-Based Phosphors

Phenothiazine is a good electron-donating group which is easily modified by bulky substituents. Therefore, using a phenothiazine unit to construct molecules with D–A–D or D–A structures can generate a spatially well-separated HOMO and LUMO. This produces an ICT state and a small ΔE_{ST}, which can accelerate the ISC process. In 2016, Bryce's group reported a number of phenothiazine-based luminophores, in which sterically bulky groups on the phenothiazine ring restrict rotation around the bond of carbon and nitrogen linking the donor and acceptor moieties (Figure 10a). In zeonex films, compounds **1** and **6** have obvious TADF. However, with increasing steric hindrance from methyl to

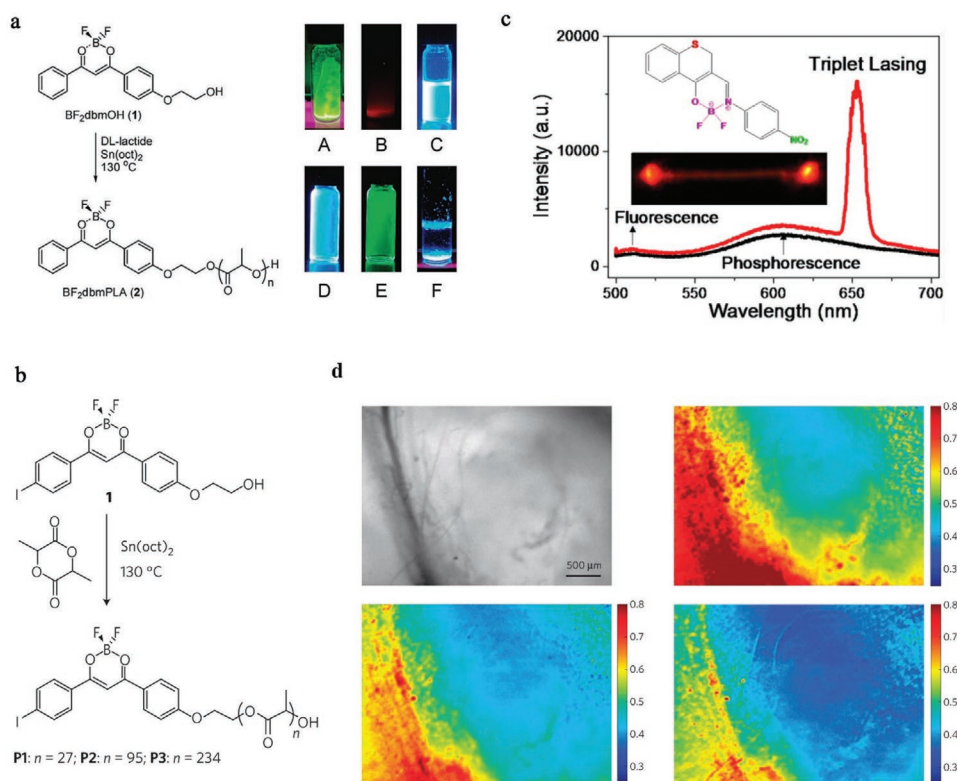


Figure 8. a) Synthesis of difluoroboron-based polymer. Insert: luminescent images under 365 nm UV light. BF₂dbmOH: A) solid-state at RT; B) solid-state at 77 K; C) CH₂Cl₂ solution. BF₂dbmPLA: D) short-lived blue fluorescence and E) phosphorescence in a thin film under nitrogen; F) particle suspension in water after 45 days. Reproduced with permission.^[61] Copyright 2007, American Chemical Society. b) Polymerization of BF₂dbm(I)PLA (P1–P3). Reproduced with permission.^[62] Copyright 2009, Nature Publishing Group. c) Triplet lasing. Reproduced with permission.^[63] Copyright 2017, American Chemical Society. d) Images of tumor hypoxia with P2 NPs. Reproduced with permission.^[41] Copyright 2009, Nature Publishing Group.

t-Bu groups on the phenothiazine rings, phosphorescence gradually dominates in the solid-state emission.^[65] They proposed that the motion of bulky, substituted molecules when aggregated is thus restricted and there is less conformational flexibility, such that electron transfer from the ¹D–¹A states to the ¹CT state is prohibited (Figure 10b). Moreover, the main non-radiative relaxation that affects T₁ is also restricted, leading to long-lived RTP under ambient conditions. In 2019, they also developed the strategy of using methoxy groups to increase the value of Φ_p in

the solid-state.^[66] As mentioned before, the methoxy groups lead to molecules with rigid D–A–D and D–A structures (Figure 10c and 10d) which promote efficient RTP properties.

3.3.3. Phenothiazine 5,5-Dioxide-Based Phosphors

In order to promote n–π* transitions and populate triplet states, Li et al. developed a number of phenothiazine-5,5-dioxide

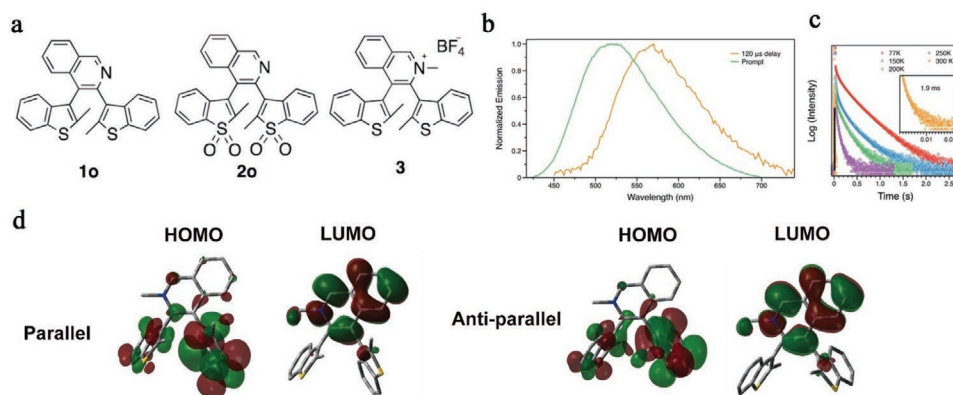


Figure 9. a) Molecular structures of **1o**, **2o**, and **3** (top). b, c) PL spectra and decays of **3** in the powder state under air. d) Frontier orbital diagrams of compound **3** in parallel and anti-parallel conformations. Reproduced with permission.^[64] Copyright 2020, The Royal Society of Chemistry.

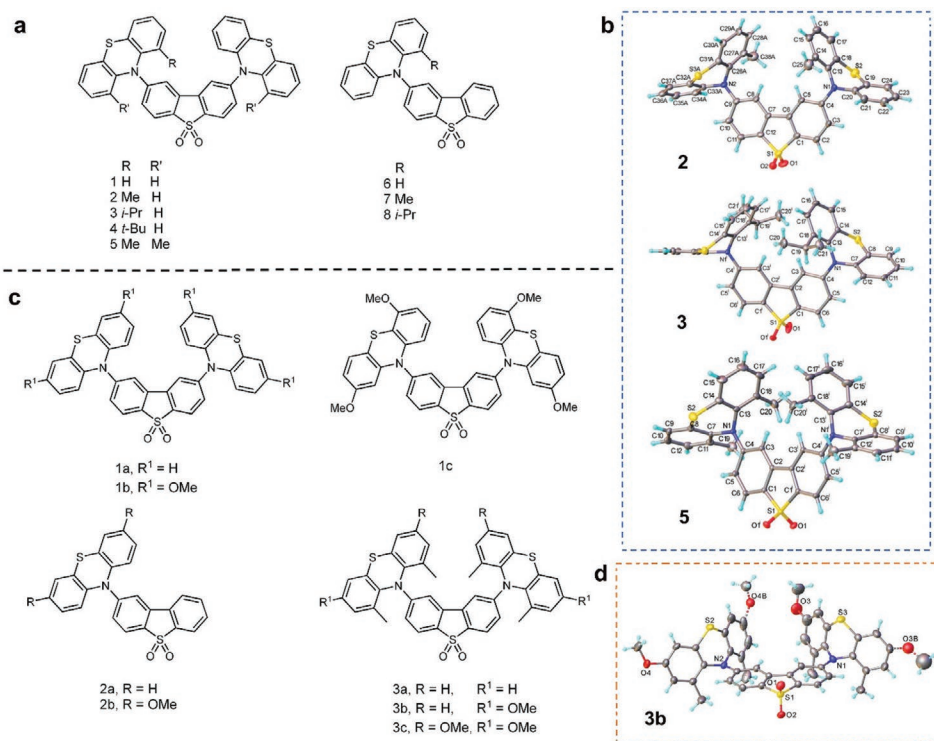


Figure 10. a) Structures of D–A–D and D–A molecules 1–8. b) Crystal structure of 2, 3, and 5. Reproduced with permission.^[65] Copyright 2016, The Royal Society of Chemistry. c) Molecular structures of 1a–1c, 2a–2b, and 3a–3c. d) Crystal structure of 3b. Reproduced with permission.^[66] Copyright 2019, American Chemical Society.

derivatives (CS–CH₃O, –CH₃, –H, –Br, –Cl, and –F),^[67] all of which displayed RTP properties with lifetimes ranging from 88 to 410 ms (**Figure 11a**). After systematic investigation of the calculation results and crystal structures, they suggest that robust π – π interactions between molecules could help in the stabilization of the T₁ state (**Figure 11b**). In addition, phosphors CS–Br, –Cl, and –F, bearing accepting groups, have more enhanced π – π interactions, compared to those (CS–CH₃O and CS–CH₃) with donor substituents, resulting in more intense RTP. They demonstrated that phosphor CS–F is a good candidate for bioimaging applications due to the long phosphorescence lifetime (**Figure 11c**). In 2019, they reported the use of an aromatic-substituted phenothiazine-5,5-dioxide with nonaromatic alkyl chains to obtain a series of CS–C_nH_{2n+1} phosphors.^[68] It is interesting that these organic RTP luminophores showed an odd-even effect with odd alkyl-substituted compounds that exhibited longer phosphorescence lifetimes than those modified with even ones (**Figure 11d**). They selected CS–C₃H₇, which shows the best RTP performance, to investigate its use in in-vivo imaging (**Figure 11e**). After subcutaneous injection of NPs of CS–C₃H₇, persistent phosphorescence was clearly observed in a living mouse with low background noise.

3.3.4. Other Types of Sulfur-Containing Phosphors

Zhang et al. developed thioether-based molecules DSP and DSQ (**Figure 12a**) which show “turn-on” RTP after treatment with AcOH or HCl vapor.^[69] The emission from the compounds

cannot be observed when irradiated by 365-nm UV. However, when exposed to acid vapor, DSPH⁺ and DSQH⁺ show bright green or yellow emission upon irradiation at RT (**Figure 12b**), which is a good example of the use in acid sensors via RTP “turn-on” properties. Theoretical calculations revealed that the lowest triplet states of DSP and DSQ are largely localized π – π^* transitions. After protonation, however, the lowest triplet states are CT transitions, resulting in strong RTP (**Figure 14c**). This “turn-on” organic RTP molecular design has potential applications for acid sensors. In 2020, Chou et al. also reported a sulfur-based photoinduced intramolecular H-bond on/off switching RTP system (**Figure 14d**).^[70] Interestingly, they observed dual RT phosphorescence bands at 550 and 685 nm in DM-7HIT. According to the identical lifetimes and calculated energies of the excited states, they excluded many possibilities for the origin of the 550 nm band such as T–T annihilation, TADF, ESIPT (excited-state intramolecular proton transfer), and a higher T₂ state. Finally, they proposed a hydrogen bond on/off mechanism which incorporates one pre-equilibrium involving two states T₁ and T₁' mainly resulting from n to π^* transitions (**Figure 14e**), leading to identical phosphorescence lifetimes at 550 and 685 nm in solution-phase. This proposed hydrogen bond on/off mechanism broadens the scope for organic RTP molecules.

3.4. Quinoxaline Derivative-Based RTP Materials

The design principles for TADF molecules bearing a D–A structure, which requires small ΔE_{ST} values and efficient ISC

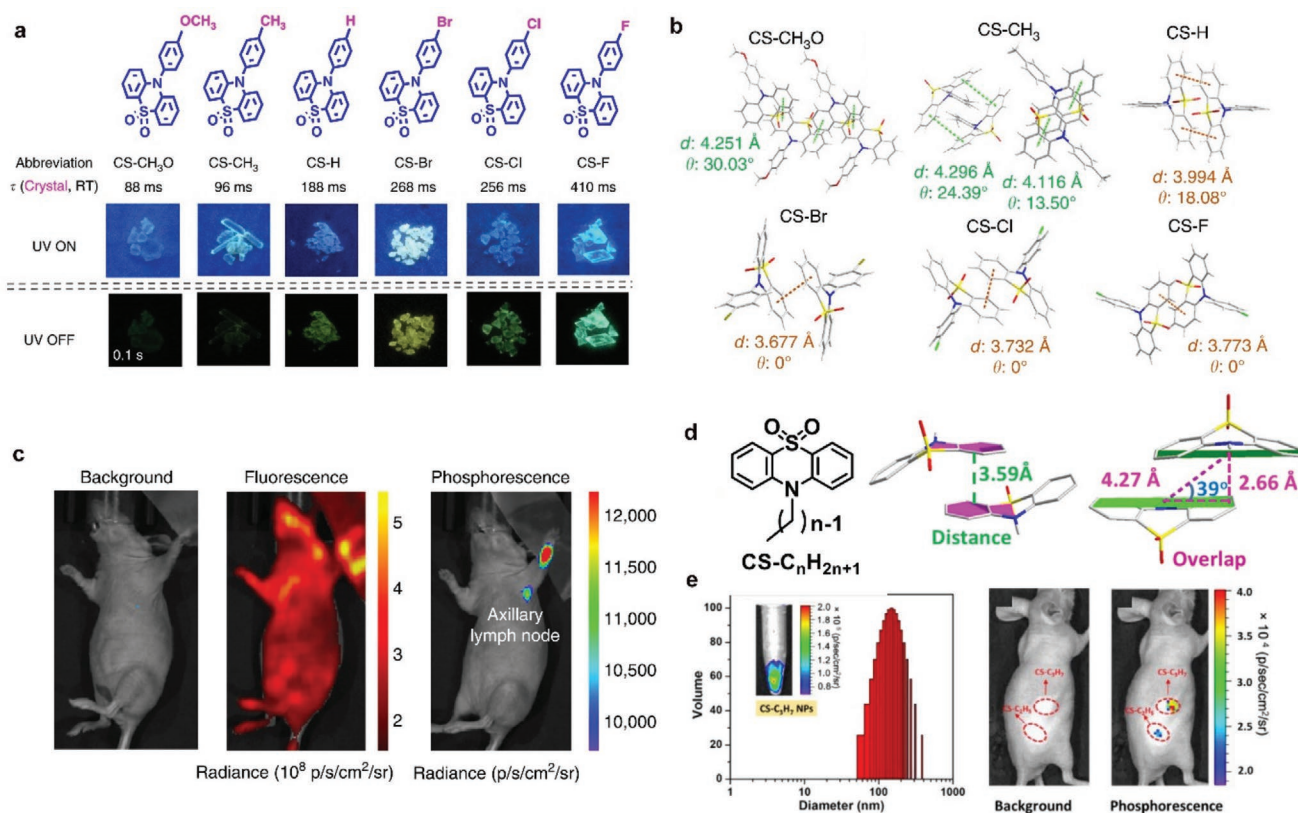


Figure 11. a) Molecular structures of the six compounds from CS-CH₃O to CS-F (top). Afterglow photographs of the six targeted molecules (bottom). b) Crystal structures of six compounds from CS-CH₃O to CS-F. c) Ultralong phosphorescence and fluorescence imaging of lymph node in living mice 1 h after the intradermal injection of CS-F NPs into the forepaw of mice. Reproduced with permission.^[67] Copyright 2018, Nature Publishing Group. d) Molecular and crystal structures used in this work. e) The left is the particle size distribution spectrum, insert: in vitro phosphorescence imaging of CS-C₃H₇ NPs. At the right are in-vivo phosphorescence imaging pictures of CS-C₃H₇ and CS-C₂H₅ NPs. Reproduced with permission.^[68] Copyright 2019, The Royal Society of Chemistry.

processes, are quite similar to the basic ones used for organic RTP molecules. In 2017, Yang's group designed a new purely organic luminophore with simultaneous TADF and RTP properties.^[71] The quinoxaline group is an electron acceptor while the phenoxazine moiety was chosen as the electron donor. Because of the well-separated HOMO and LUMO (Figure 13a), ΔE_{ST} of DBQPXZ is as low as 0.0863 eV while the corresponding calculated value is 0.0871 eV. In the crystalline state, the band at 564 nm is ascribed to organic phosphorescence of which the lifetime is 3.2 ms at room temperature (Figure 13b,c). Interestingly, when the temperature is below 170 K, the S₁ to T₁ transition dominates the decay process. When the temperature is above 170 K, TADF emission is the main component. Moreover, the external quantum efficiency of a fabricated OLED device can reach up to 16.8%. In 2018, Ma et al. reported an azaromatic DPPZ based on phenazine (Figure 14a), for which the authors found single-molecule white light emission (SMWLE) which they explained with a dual RTP emission, T₂ → S₀ and T₁ → S₀.^[72] When the time gate is set to 160 μs, the nanosecond lifetime of DPPZ disappears completely, and only the long lifetime belonging to dual phosphorescence (T_n and T₁) appeared in the spectrum (Figure 14b). In addition, the emission band between 480 and 530 nm is assigned to the T₂ state and almost disappears when the delay timescale reaches 1.4 ms.

3.5. Siloxy Group-Induced RTP Materials

While elements such as nitrogen, oxygen, and sulfur bearing lone pairs are commonly used in the molecular design of RTP materials, silicon is rarely employed in phosphorescent luminophores. In 2016, Hasobe et al. reported siloxy-substituted benzene derivatives 1a–1c (Figure 14c). The phosphorescence lifetimes are ≈76.0 to 98.3 ms and they show outstanding luminescence quantum yields of 46% to 64%.^[73] By crystal structure analysis, they found multiple intermolecular interactions which efficiently reduce intramolecular motion, thereby suppressing nonradiative decay to a large extent. Calculations revealed that the conjugation between silicon to carbon σ-orbitals and the n-orbital of the siloxy moiety can stabilize the T₁ state, which explains the remarkably high RTP performance. According to the proposed mechanism, the positions of silicon and carbon atoms connected to the oxygen atom of the ether do not influence the stabilization of the T₁ state through σ–n conjugation (Figure 14d). Therefore, they also investigated a series of silyl-methoxy benzene derivatives 2a–2f.^[74] They found that 2a–2f not only exhibits intense RTP in the crystalline state, but shows efficient RTP when doped in PMMA films which were prepared and measured under vacuum. Moreover, the phosphorescence of PMMA films of 2 responds quickly to

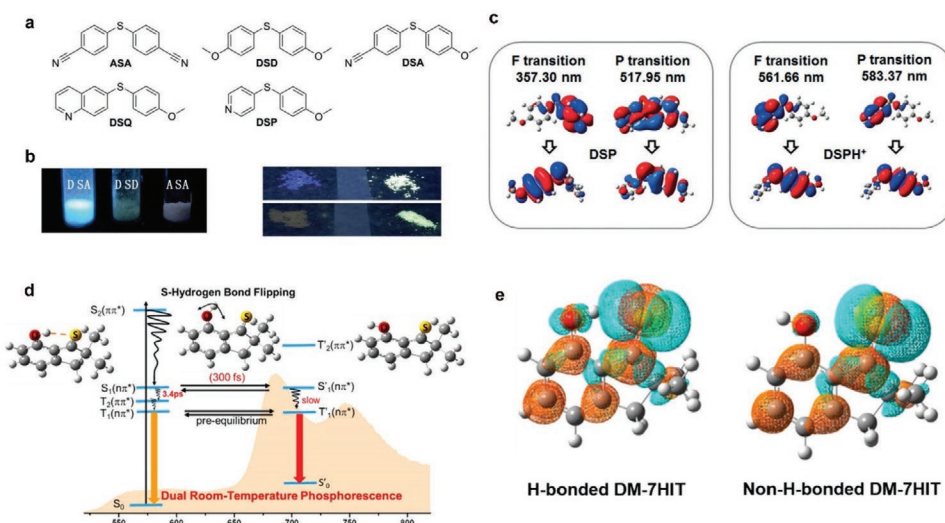


Figure 12. a) Molecular structures of ASA, DSD, DSA, DSQ, and DSP. b) PL images of crystalline DSA, DSD, and ASA under 365-nm UV light (left). Photographs displaying PL changes of crystalline DSQ and DSP before and after exposure to acetic acid vapor (right). c) Molecular orbital diagrams showing fluorescence (F, lowest singlet-state) and phosphorescence (P, lowest triplet-state) transitions for DSP/DSPH⁺ pair. Reproduced with permission.^[69] Copyright 2018, Wiley-VCH. d) Schematic energy diagram of the mechanism of H-bond hopping for DM-7HIT. e) The calculated HOMO and LUMO of H-bonded and non-H-bonded DM-7HIT. Reproduced with permission.^[70] Copyright 2019, American Chemical Society.

oxygen and is thus a potential candidate for application as an oxygen sensor.

3.6. Carbazole-Based RTP Materials

RTP phosphors based on carbazole have been widely investigated in recent years.^[75] However, in 2020, Liu et al. proved that the presence of an isomeric impurity in commercial carbazole

leads to enhanced RTP even with a concentration of less than 0.5 mol%,^[25] as the isomeric impurity can cause obvious differences in the RTP lifetime and quantum yield. Therefore, we suggest that the reported carbazole-based RTP materials which were prepared directly from commercial carbazole should be carefully reexamined. On the other hand, reported research already confirmed that carbazole derivatives tested for purity exhibit RTP. In order to make comparisons with the corresponding carbazole isomer, Tang et al. investigated TCz-F, TCz-H, and TCz-OH (Figure 15a) which were synthesized from commercial/lab carbazole through S_NAr reactions.^[26] This provided insight into the push-pull electronic effect on photophysical behavior. Lab-made TCz-OH-Lab only shows fluorescence while TCz-F-Lab and TCz-H-Lab exhibit obvious RTP in the solid-state with a phosphorescence lifetime as long as 48.6 and 29.9 ms and quantum yield up to 0.8% and 0.7%, respectively. The isomer did have a great influence on the RTP properties. On one hand, the phosphorescence emissions of TCz-F-Lab and TCz-H-Lab were blueshifted by ≈40 nm compared to corresponding commercial compounds. On the other hand, both the phosphorescence lifetimes and quantum yields were dramatically enhanced, indicating that the effect of the isomer should not be neglected in carbazole-related phosphors. Due to the strong blue fluorescence and efficient RTP of TCz-F-Cm, it was successfully applied as an emitter material in an OLED device to generate white-light emission with CIE coordinates of (0.357, 0.317) at a current density of 3.6 mA cm⁻² (Figure 15b). Also in 2020, Aakash et al. designed carbazole-based phosphor **3a**, functionalized by a phenylmethanone group (Figure 16a) which has an ultralong phosphorescence lifetime of over 4.1 s and a high quantum yield of up to 11%, by controlling the molecular packing in the crystalline state.^[76] In addition to the small ΔE_{ST} to facilitate the ISC process, and intermolecular interactions to suppress nonradiative decay, the existence of dense helical arrays in the aggregated solid of **3a** significantly stabilizes the

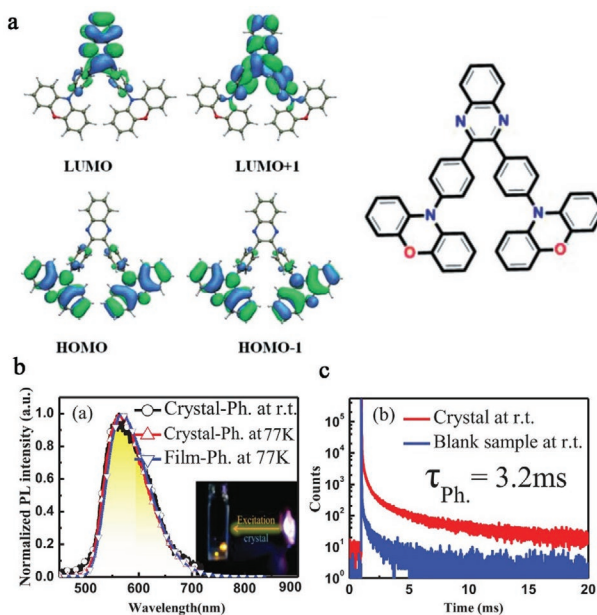


Figure 13. a) Molecular structure of DBQPXZ and its frontier orbitals. b) Normalized phosphorescence and c) Transient PL decay spectra of DBQPXZ. Reproduced with permission.^[71] Copyright 2017, Wiley-VCH.

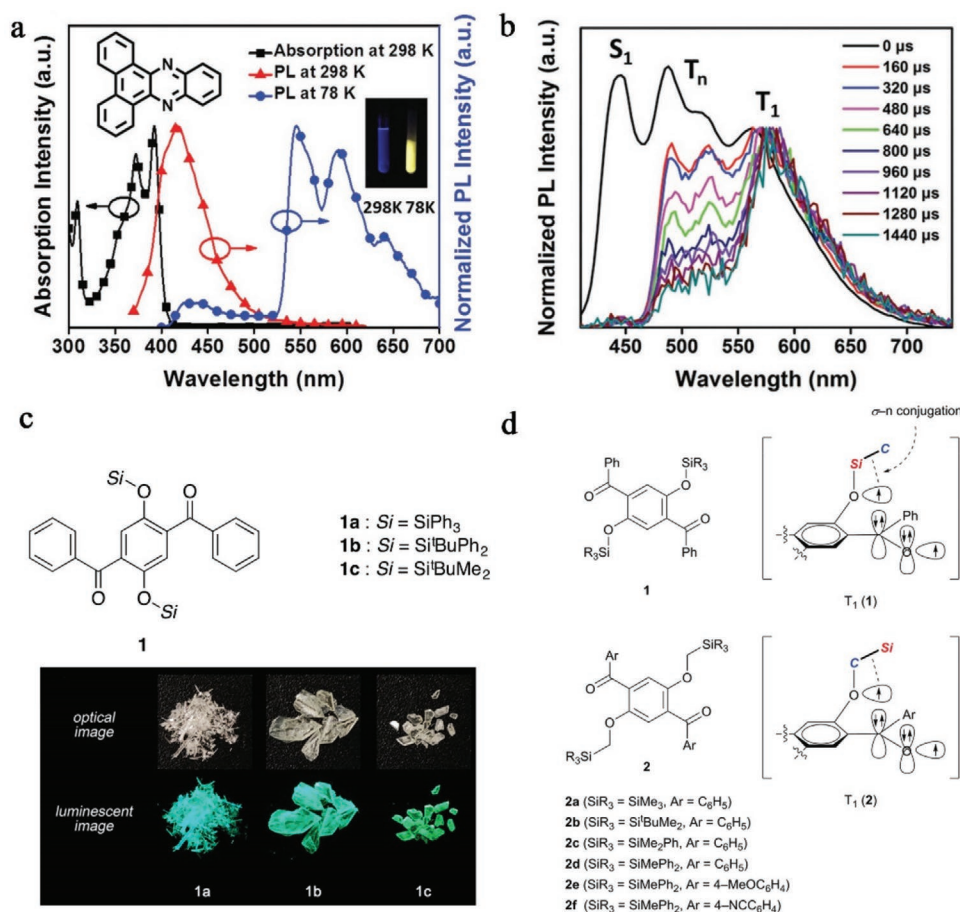


Figure 14. a) Chemical structure, absorption, and emission spectra of DPPZ in THF solution at 298 and 78 K. b) Normalized PL spectra of DPPZ as a neat powder. Reproduced with permission.^[72] Copyright 2018, Wiley-VCH. c) Molecular structures of 1,4-dibenzoyl-2,5-bis(siloxy)benzenes **1a**–**1c** (top) and luminescent images of crystals (bottom). Reproduced with permission.^[73] Copyright 2016, American Chemical Society. d) Chemical structures and orbital descriptions of the T_1 states of **1** and **2**. Reproduced with permission.^[73] Copyright 2018, The Royal Society of Chemistry.

triplet state, resulting in the long phosphorescence lifetime (Figure 16b). No helical arrays and only loose packing modes in the crystalline assembly were observed for **1**, **2**, and **3b**–**3e**. Therefore, they show weaker RTP than **3a**. Very recently, Li's group also synthesized two carbazole-based RTP luminophores PTCz and CCz (Figure 16c) substituted by a phthalide (PT) moiety and by a typical C=O unit, respectively.^[77] The butterfly-like molecule PTCz showed a much longer phosphorescence lifetime (τ_p) of 810 ms and quantum yield (Φ_p) of 5.1% while the τ_p value of its corresponding carbonyl-substituted molecule CCz is only 12.1 ms. In crystals, the PT unit enabled PTCz to adopt the desired strong packing mode which produced intense intermolecular interactions. In addition, the neighboring acceptor (PT unit) and donor (Cz group) facilitate ICT, enabling transitions between the singlet and triplet states (Figure 16d). They also provided an example of the application of PTCz in anti-counterfeiting. Upon turning off the UV light, only "F" made from PTCz showed the yellow afterglow in the original pattern "E" (Figure 16e). In 2019, Wu et al. reported carbazole-based difluoroboron β -diketonates H-, Br-, and I-NpCzBF₂ which can assemble into NPs in water (Figure 17a).^[78] Carbazole is designed to act as the electron-donating part while difluoroboron is used as the electron-accepting unit. Interestingly,

these phosphors can be excited via two-photon in the NIR region because of the two-photon absorption ability of BF₂bdk moieties. By utilizing NIR irradiation, these carbazole-based phosphors were applied in bioimaging (Figure 17b). In addition, the heavy atoms (Br and I) speed up the ISC by enhancing the SOC, resulting in a better performance in Br-NpCzBF₂ (τ_p = 0.58 ms) and I-NpCzBF₂ (τ_p = 0.56 ms) compared to H-NpCzBF₂ (τ_p = 0.13 ms). Calculations reveal that intermolecular charge transfer in the dimer structures decreased greatly compared to the isolated molecule, leading to an enhanced ISC process (Figure 17c).

3.7. Other RTP Materials with Unusual Structures

Quinoxalines, phenothiazines, boronic esters, and amides and their derivatives are typically utilized as single-component organic phosphors. However, there are a few RTP materials which are not based on these common structures. Below are a few examples selected for discussion. In 2018, Tang et al. designed and synthesized five different heavy halide-substituted organic salts based on phenyl oxazolium (TPO-I, -Br, -Cl, -F, and -P), which are highly emissive under UV light with

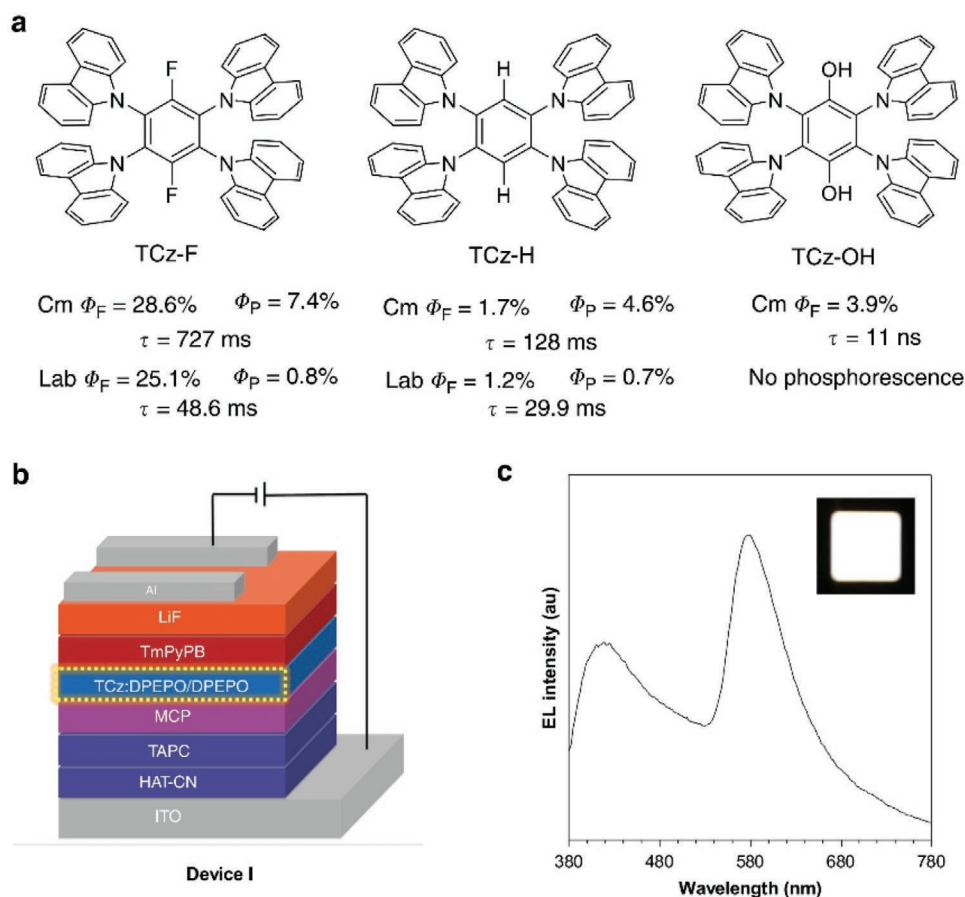


Figure 15. a) Molecular structures and photophysical properties. b) Configuration of OLED. c) The EL spectrum of device I at a current density of 3.6 mA cm^{-2} . Reproduced with permission.^[26] Copyright 2020, Nature Publishing Group.

phosphorescence lifetimes ranging from 48 to 706 μs .^[79] Crystal structures and results of calculations indicate that interactions between the negative charge of the halide and positive charge of the aromatic ring improve SOC and increase the ISC rate. These so-called anion- π^* interactions involving halide atoms represents a new design for RTP luminophores. Among the five phosphors, in the solid-state, TPO-Br exhibits SMWLE with a combination of blue fluorescence and yellow RTP (Figure 18a). In addition, the white light color could also be obtained by changing the ratios of components between TPO-I and -Cl or TPO-I and -P. They successfully doped TPO-Br in PEG and demonstrated its application as a white light display and in 3D printing. In 2019, Bechtold et al. reported the non-planar homotrioxene phosphor **8** (Figure 18b) which was synthesized by dehydrative cyclotrimerization of 1-tetralone at high temperature with TiCl_4 .^[23] The temperature-dependent emission spectrum showed a strong emission at 566 nm. The phosphorescence lifetime reaches 0.38 s and the value of Φ_P is up to 5.6% under ambient conditions in the solid-state. In addition to phosphorescence, there is also a delayed fluorescence peak at 412 nm induced by TTA, as indicated by its temperature and concentration dependence. Although there is no heavy atom or heteroatom bearing lone pairs to enhance ISC, calculations suggested that the twist between one central benzene ring and the three outer benzenes of **8** causes a change of angular momentum associated with electronic transitions which are

necessary for SOC. In addition, the high triplet energy reduces nonradiative decay pathways. In the same year, Huang's group reported a series of indolo[3,2-b]carbazole analogs (Figure 18c). The RTP maxima of the analogs vary from 442 to 623 nm and the related phosphorescence lifetimes range from 2 to 759 ms.^[80] Theoretical calculations suggest the absence of an ISC process in the isolated molecule despite the narrow energy gap (Figure 18d). When aggregated, T-shaped dimers form hydrogen to π interactions which induce ICT between indolyl and phenyl groups leading to a high radiative decay rate. Furthermore, the calculated orbital coupling element of Ben-H for T_1/S_0 (1.25 cm^{-1}) is much larger than that in the isolated molecule ($\ll 10^{-2} \text{ cm}^{-1}$) also demonstrating the importance of aggregation. Finally, the influence of C-H $\cdots\pi$ interactions suppressing molecular thermal rotation and vibration in the crystal cannot be neglected.

4. Multi-Component RTP

4.1. RTP from Host-Guest Systems

4.1.1. Trap/DeTrap Mechanism

Host-guest systems are one of the most important categories of multi-component RTP phosphors. Among them, a number of

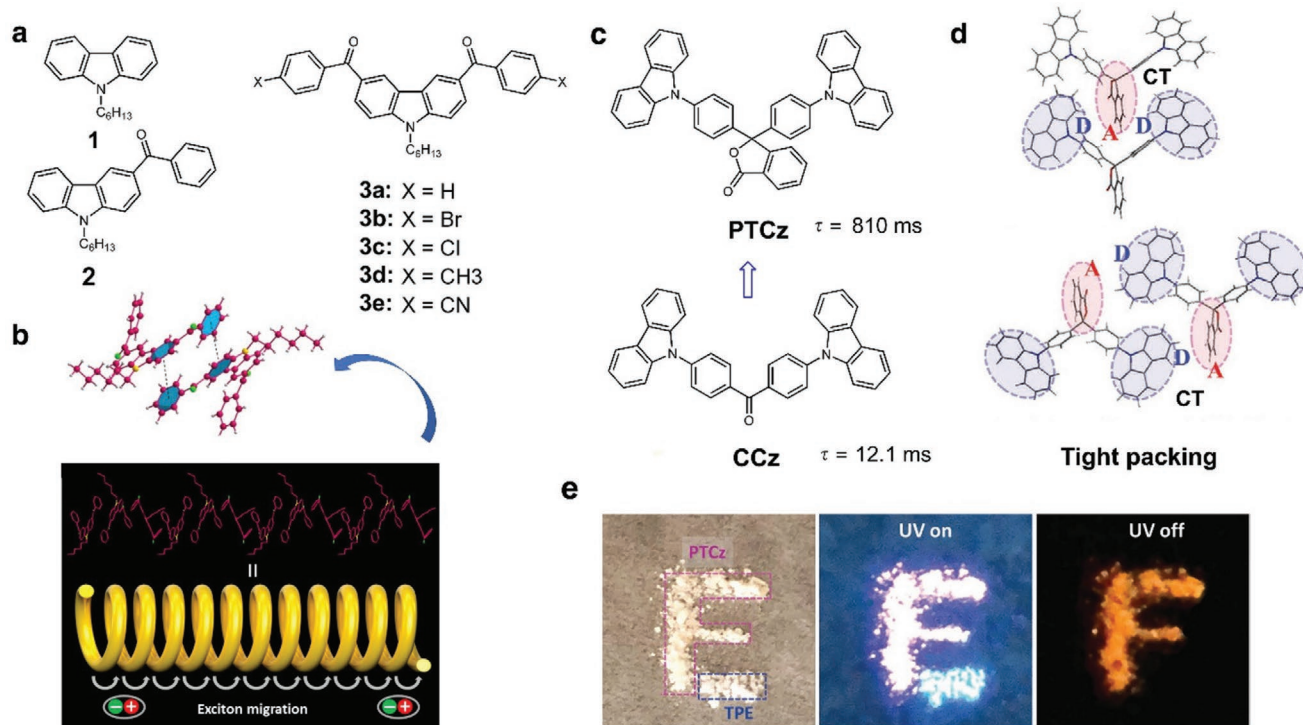


Figure 16. a) Chemical structures of compounds **1**, **2**, and **3a–3e**. b) Schematic of the helical array of **3a** leading to triplet exciton migration, insert: π - π interaction between the adjacent molecules. Reproduced with permission.^[76] Copyright 2020, Wiley-VCH c) Molecular structures of PTCz and CCz. d) Tight packing mode in the crystals. e) Photographs of the letter “E” containing the pattern “F”, demonstrating the potential application of the PTCz materials in anticounterfeiting. Reproduced with permission.^[77] Copyright 2021, Wiley-VCH.

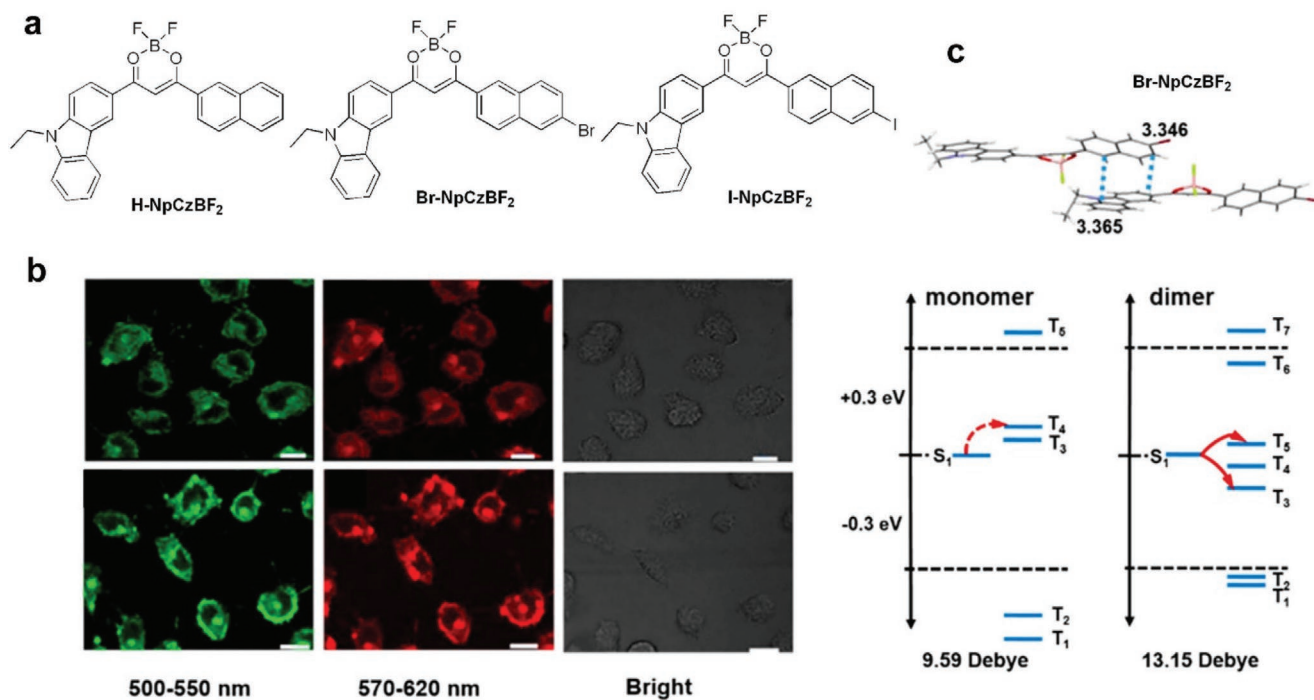


Figure 17. a) Molecular structures of H-NpCzBF₂, Br-NpCzBF₂, and I-NpCzBF₂. b) Confocal luminescence images of HeLa cells incubated with BrNPs. c) Intermolecular packing in Br-NpCzBF₂ crystal; the energy levels of monomer and dimer of Br-NpCzBF₂ based on TD-DFT (B3LYP/6-31G*) calculations.^[78] Copyright 2019, American Chemical Society.

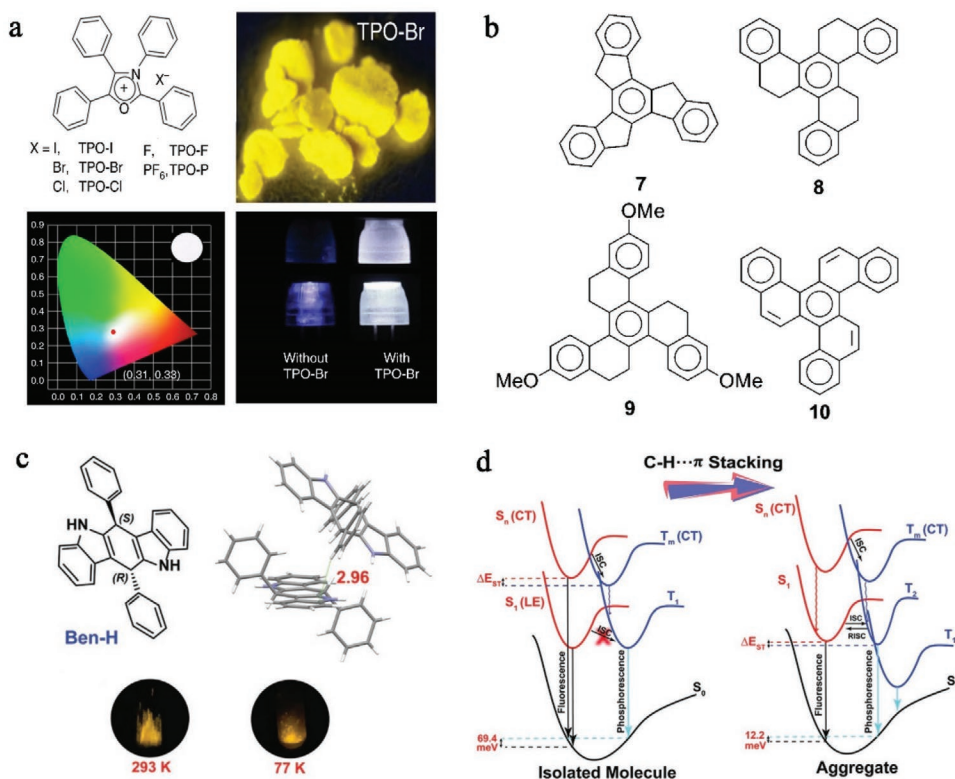


Figure 18. a) Chemical structures of TPO-I, -Br, -Cl, -F, and -P (top left). Photographs of TPO-Br under UV light (top right). CIE 1931 coordinates from the TPO-Br-based PEG film (2%, m/m, bottom left). Luminescent images of 3D printed lampshades irradiated at 365 nm without and with TPO-Br (bottom left). Reproduced with permission.^[79] Copyright 2018, Nature Publishing Group. b) Planar and twisted rigidified derivatives of triphenylbenzene. Reproduced with permission.^[23] Copyright 2019, Wiley-VCH. c) Molecular structure of Ben-H and the C-H... π interaction in Ben-H-DMSO. d) The proposed energy level diagrams for Ben-H in single-molecule and aggregated state. Reproduced with permission.^[80] Copyright 2019, Wiley-VCH.

host-guest systems are related to the trap/detrap mechanism, which requires efficient photo-induced charge separation and charge recombination processes. In 2017, Adachi's group chose molecule TMB (guest) as the donor with a very stable radical cation, and PPT (host) as the strong acceptor (Figure 19a).^[81] When photoexcited, charge-transfer occurs between TMB and PPT. The radical anions produced diffuse until they encounter a TMB radical cation. During the slow recombination process, phosphorescent emission is generated (Figure 19b). The phosphorescence duration of a fabricated 1 mol% TMB/PPT film can last for more than 5000 s with an excitation time of 180 s at 300 K. In subsequent work,^[82] they systematically studied the RTP properties using three different donor molecules (TMB, DMDTB, and TTB) and the same acceptor PPT (Figure 19c). The RTP performance is greatly influenced by the energy gap between ^1CT (lowest singlet excited state of the exciplex) and $^3\text{LE}_D$ (the lowest triplet excited state of the donor). They demonstrate that the large energy gap for populating the ^3LE excitons, which inhibits the charge-transfer process, leads to a reduced quantum efficiency of phosphorescence.

Organic RTP materials based on carbazole (Cz) and its derivatives recently have been widely developed. In 2020, Liu et al. successfully isolated and identified the impurity which was an isomer of Cz, namely 1H-benzof[*f*]indole (Bd), from a commercially available Cz source.^[25] Next, they prepared two kinds of Cz starting materials. One was from commercially

available Cz obtained from TCI (Tokyo Chemical Industry, TCI-Cz) while the other Lab-Cz was prepared from 2-amino-biphenyl (Figure 19d). With the two Cz sources, they checked two reported RTP phosphors CPhCz and DPhCzT, and found that although the crystals have the same unit cells, TCI-CPhCz and TCI-DPhCzT showed RTP, while Lab-CPhCz and Lab-DPhCzT showed no emission upon turning off the UV light (Figure 19e). Interestingly, the impurity Bd itself does not exhibit RTP in the crystalline state, so they performed doping experiments with CPhCz and DPhCzT and their corresponding isomeric impurities CPhBd and DPhBdT at 0, 0.5, 1.5, 10, and 100 mol%, respectively. All doped systems examined exhibited obvious RTP with different lifetimes and quantum yields. Even 0.01 mol% CPhBd and DPhBdT still showed RTP. They proposed that Cz and Bd have different electron-donating abilities and induce charge-separated states which can act as good triplet energy traps (Figure 18f). Importantly, they also speculate that, in addition to carbazole systems, impurity issues may also exist with dibenzothiophene and dibenzofuran derivatives. Very recently, Ma et al. also reported RTP induced by trace components.^[83] They incorporate two host molecules 1BBI and DIB with seven guest molecules to form bicomponent RTP systems (Figure 20). The RTP quantum yield of 1BBI/4BBI is as high as 74.2% while the lifetime of DIB/DMQI can reach up to 430 ms. This work provides additional insight into the impact of impurities on RTP properties.

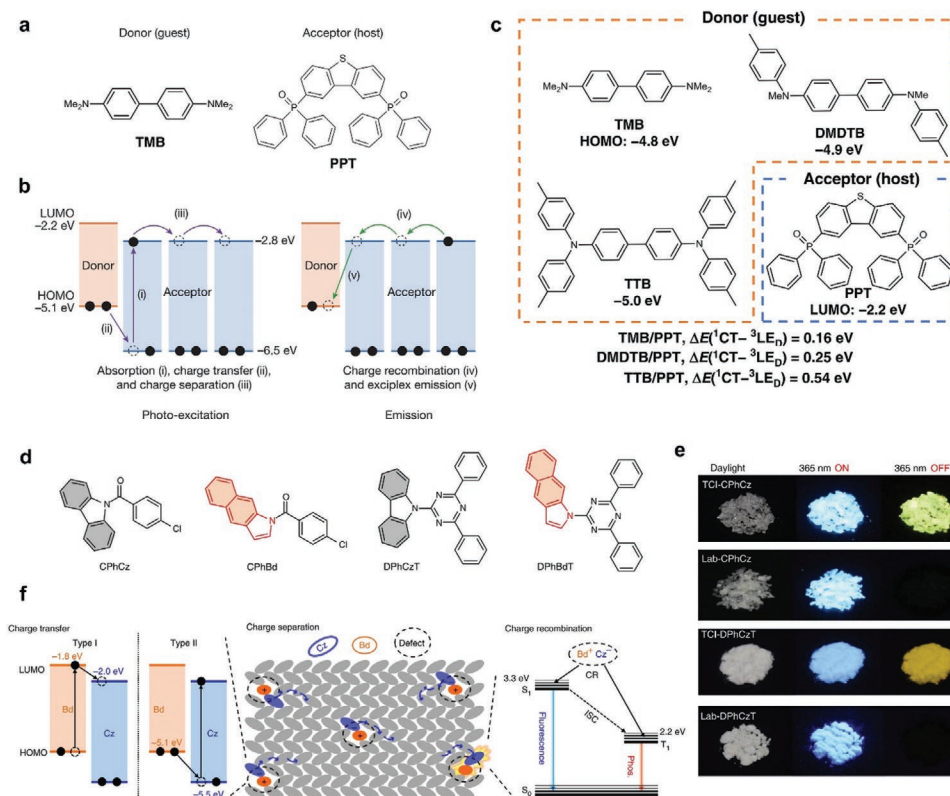


Figure 19. a) Chemical structures of TMB and PPT. b) Proposed mechanism of RTP. Reproduced with permission.^[81] Copyright 2017, Nature Publishing Group. c) Chemical structures and HOMO or LUMO energy levels of the three electron donors (TMB, DMDTB, and TTB) and the electron acceptor (PPT). Reproduced with permission.^[82] Copyright 2020, Nature Publishing Group. d) Molecular structures of CPhCz, CPhBd, DPhCzT, and DPhBdT. e) Images of TCI- and laboratory synthesized CPhCz and DPhCzT crystalline powders before and after UV light irradiation. f) Proposed mechanism of RTP. Reproduced with permission.^[25] Copyright 2020, Nature Publishing Group.

4.1.2. $n-\sigma^*$ Orbital Interaction

In addition to bicomponent systems for persistent RTP governed by the trap/detrap mechanism, some unintended discoveries also inspired researchers to explore the reason for their observations. Zhang's group unexpectedly found that a trace amount of side product X generated by a side reaction with the DMF solvent could induce persistent RTP when doped in the host BrBID (Figure 21a).^[84] The quantum efficiency of the bicomponent system X/BrBID is up to 25.4% with a lifetime of 48 ms. After excluding the possibility of a single heavy atom effect, they proposed that in the crystalline matrix, molecule X could replace the position of BrBID which causes an $n-\sigma^*$ orbital interaction between a Br atom and an NMe₂ group, thus enhancing the SOC (Figure 21b). This work not only provides a new view on persistent RTP from bicomponent systems but also confirms the role of trace impurities and their dramatic influence on the observed RTP phenomenon, which might be mistaken for single molecular behavior.

4.1.3. Restriction of Non-Radiative Decay

This strategy usually introduces strong intermolecular interactions into designed system, such as hydrogen bonding which

could restrict and prevent molecular rotations and vibrations to a large extent, and thus reduce the nonradiative pathways and boost the phosphorescence efficiency. In 2011, Kim et al. reported an emitter/host system with ambient phosphorescent quantum yields reaching 55% by combining three concepts: the heavy atom effect, aromatic carbonyls, and halogen bonding.^[85] The emitter Br6A suffered from luminescent quenching with moderate phosphorescence upon aggregation (Figure 22a,c). When the emitter, a brominated aromatic aldehyde (Br6A), is doped into

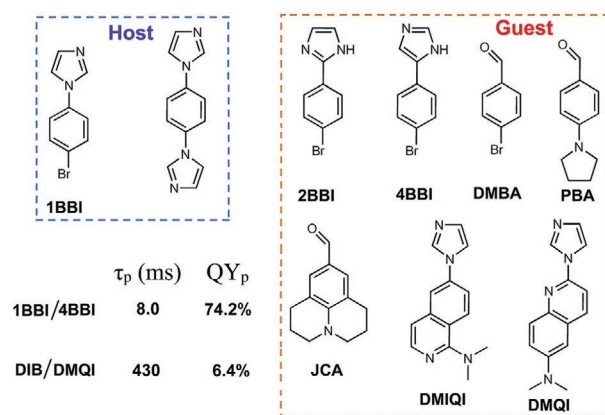


Figure 20. Molecular structures of selected host and guest molecules.

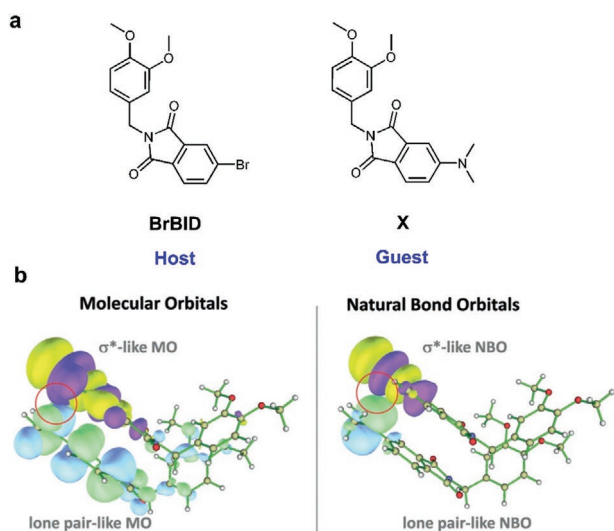


Figure 21. a) Molecular structures of BrBID and X. b) Molecular orbitals and natural bond orbitals of the proposed BrBID and X model in the crystal. Reproduced with permission.^[84] Copyright 2020, Wiley-VCH.

the host crystal, a dibrominated analog (Br6), self-quenching of the isolated Br6A molecules is successfully prevented. Therefore, the overall quantum yield is largely enhanced (Figure 22b,d). As the experiment results indicate, the brominated aromatic aldehyde emitters always show the best RTP performance when

doped into a matrix of their dibrominated analogs. Moreover, the aldehyde groups are close to bromine atoms, which promotes the population of triplet states and activates phosphorescence emission. In addition to Br6A/Br6 system, the authors also examined the doping effect of the emitters Br(5-8)A and the hosts Br(5-8). These systems display phosphorescence quantum yields ranging from 9% to 55% (Figure 22e,f).^[86]

In 2013, Hirata et al. successfully achieved blue-green-red persistent host-guest RTP materials of which the phosphorescence lifetime is as long as 1 s and the quantum efficiency is as high as 10% under ambient conditions (Figure 23a,b).^[87] The secondary amino-substituted highly deuterated aromatic hydrocarbon was the guest while the hydroxy steroid was selected as the host to minimize the triplet quenching rate caused by oxygen permeation and diffusional motion. This is achieved by the introduction of a rigid matrix. According to the design strategy, they also developed a reversible recording material, which responds to heating by utilizing Dye 1 as the guest, cholesterol as the host matrix, and a phenol derivative THEB as the dispersant (Figure 23c).^[88] The recording state was achieved by exposing the host and guest system to UV light. The resulting blue-green phosphorescence can be completely erased by heating the sample to 90 °C for 1 min. Recovery can be achieved by heating the sample to 150 °C. By continuously repeating the process of recording and erasing, a reversible thermal recording material was demonstrated (Figure 23d). In 2016, the authors applied the host-guest afterglow system in OLED devices, which gave a maximum external quantum efficiency

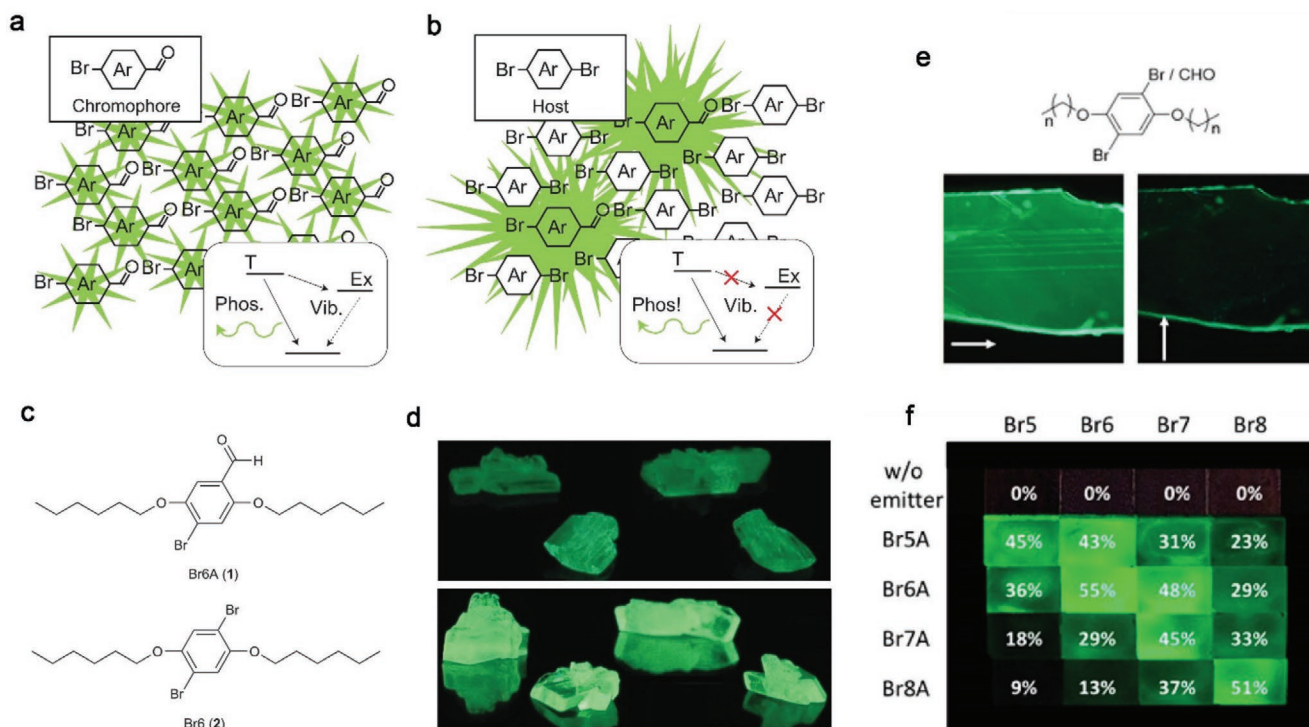


Figure 22. a) The chromophore is a brominated aromatic aldehyde. b) The host is a dibrominated analog of the chromophore. c) Molecular structures of Br6A and Br6. d) Images of crystalline Br6A and Br6 under 365 nm irradiation. Reproduced with permission.^[85] Copyright 2011, Nature Publishing Group. e) Chemical structures of Br(5-8)A and Br(5-8). Polarized phosphorescent images from a thin Br6A/Br6 crystal. f) Photograph of drop cast crystals made of host and guest molecules irradiated under 365 nm irradiation. Reproduced with permission.^[86] Copyright 2014, American Chemical Society.

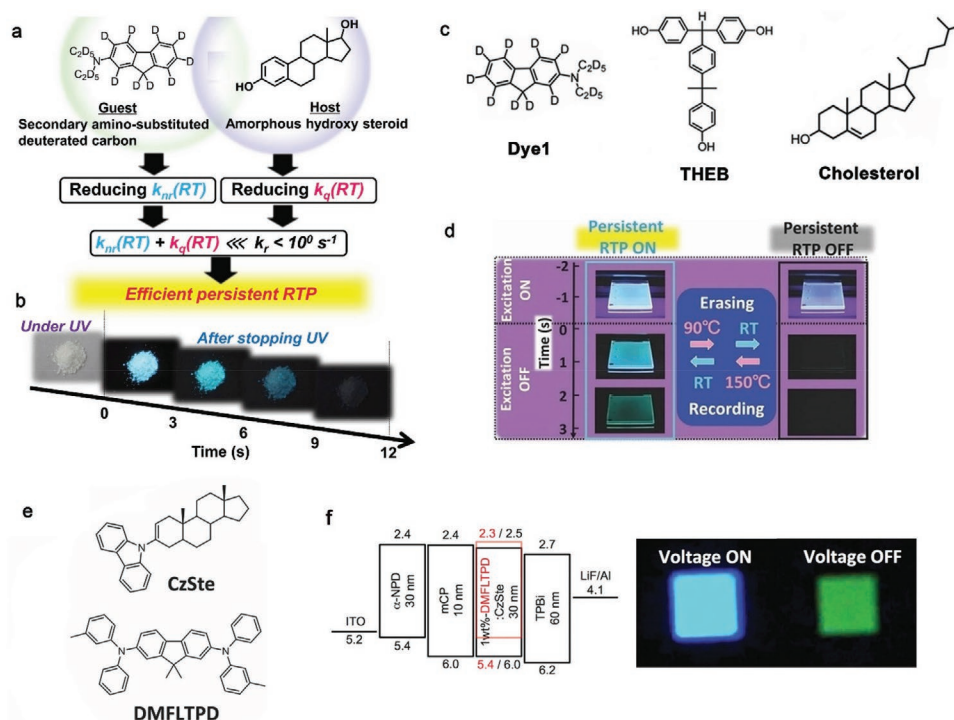


Figure 23. a) Material design for guest and host structures. b) Afterglow photographs. Reproduced with permission.^[87] Copyright 2013, Wiley-VCH. c) Chemical structures of compound 1, THEB, and cholesterol. d) Reversible thermal recording and erasing using persistent RTP. The recording material is composed of 1.0 wt% 1, 9.0 wt% THEB, and 90 wt% cholesterol. Reproduced with permission.^[88] Copyright 2013, Wiley-VCH. e) Chemical structures of CzSte and DMFLTPD. f) OLED structure showing energy levels in eV (left) and photographs of EL during and after electrical excitation of a device containing CzSte as a host (right). Reproduced with permission.^[89] Copyright 2016, Wiley-VCH.

(η EQE) of $\approx 1\%$.^[89] CzSte acts as a host and DMFLTPD-d36 was selected as an emitter in co-deposited films, achieving persistent RTP ($\tau_p = 0.61$ s) (Figure 23e). Using the DMFLTPD-d36/CzSte system as the emitter layer in OLEDs, the device showed green after glow phosphorescence ($\tau_p = 0.39$ s) (Figure 23f). They proposed that the hydrophobic steroid moiety of CzSte provides strong intermolecular interactions and forms a rigid host matrix, prohibiting molecular movements to some extent and suppressing nonradiative pathways of the guest molecules.

In 2016, Wang and coworkers developed a host-guest system with a unique greenish RTP which could last almost 1 s under ambient conditions.^[90] They inserted the guest *N*-phenyl-naphthalen-2-amine (PNA) into the host 4,4'-dibromobiphenyl (DBBP) with a mass ratio of 1:100 (Figure 24a). The Φ_{PL} value of the PNA/DBBP-doped sample was up to 30%, in which phosphorescence contributes 53% of the total emission, resulting in a very high phosphorescence quantum yield ($\Phi_p = 17\%$) (Figure 24b). Their study indicates that the host DBBP crystal serves as a rigid matrix, which isolates the emitter molecules and avoids emission quenching by efficiently reducing nonradiative decay. In 2018, Fu et al. tried doping two β -iminoenamine-BF₂ derivatives as guests (S-2CN and S-2I) into a 4-iodoaniline host (I-Ph-NH₂, Figure 24c) realizing bright red RTP emissions under ambient conditions.^[91] It was proposed that strong hydrogen bonding in the crystal of the host-guest system contributes to the efficient RTP. Interesting, S-2I/I-Ph-NH₂ is responsive to HCl vapor. Upon exposure to HCl, the existing hydrogen bonding of S-2I \cdots I-Ph-NH₂ transformed into I-Ph-

NH₂·HCl and the red RTP emission is turned off. Because a cyano group has a stronger electron-accepting ability, S-2CN/I-Ph-NH₂ still retains its bright RTP emission. According to the above observations, the host-guest doped systems are potential candidates for applications in bioimaging and anti-counterfeiting materials. In the same year, Tian and coworkers designed a host-guest system which exhibits multicolor emission, from yellow to purple and even shows white light emission.^[92] The guest is a linear blue-fluorescent AC bearing a coumarin moiety while the host is a phosphorescent β -cyclodextrin derivative BrNp- β -CD (Figure 24d). UV-Vis absorption spectra revealed that the host-guest complex interacted in a 1:1 stoichiometry. When the host-guest complex with varying ratios was excited at different wavelengths, the PL emission, and the CIE coordinate values continuously changed. The CIE coordinates (0.29, 0.33) of white-light emission were achieved when the host BrNp- β -CD was doped with 0.1 equivalent of AC and excited at 295 nm. The coordinates are quite similar to the standard white color value (0.33, 0.33). This work provides a new method in the search for pure white-light emitting materials.

4.1.4. Cluster Exciton (Transient State)

In 2019, Tang et al. selected PCP, PA, and 1,2-DCB as host matrices while 1,8-naphthalic anhydride NA (Figure 25a) was used as the guest.^[93] Both host and guest molecules are electron-deficient in order to prevent self-quenching from PET

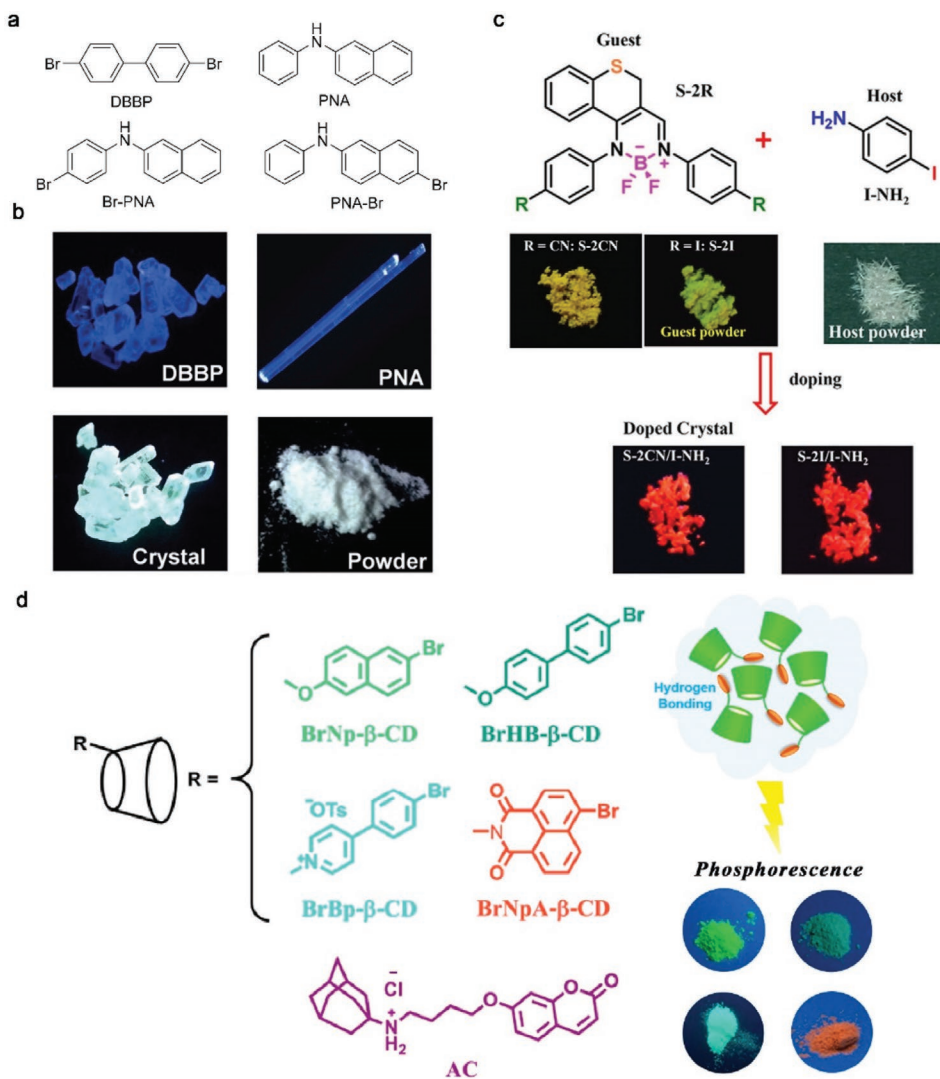


Figure 24. a) Molecular structures of host and guest. b) Images of crystalline DBBP, PNA, PNA doped DBBP (1% mass ratio), and PNA/DBBP (1% mass ratio) irradiated at 365 nm. Reproduced with permission.^[90] Copyright 2016, Wiley-VCH. c) Chemical structures of S-2CN, S-2I, and I-Ph-NH₂. Photographs of host powder crystals under ambient light; images of guest powder (top) and doped system (bottom) under 365 nm irradiation. Reproduced with permission.^[91] Copyright 2018, Wiley-VCH. d) Molecular structures of RTP emissive BrNp-, BrHB-, BrBp-, and BrNpA-β-CD and guest molecule AC. Reproduced with permission.^[92] Copyright 2018, American Chemical Society.

(photo-induced electron transfer). The phosphorescence lifetime of the doped system can reach 600 ms with a total quantum yield of over 20%. According to femtosecond transient absorption spectra, a small amount of guest molecules in the mixture can substantially enhance the rate of ISC of the host. Moreover, they proposed that cluster excitons formed by neighboring host and guest molecules produced transient species, which can be experimentally detected and then immediately relax to a stable localized triplet state of the guest (Figure 25b).

4.2. RTP from Supramolecular Systems

4.2.1. RTP from Purely Organic Materials in Polymer Matrices

Doping organic materials into polymer films is also a popular method to realize efficient RTP, as the polymer not only

provides a rigid environment but also forms intermolecular interactions with the embedded organic molecules. In 2013, Kim's group reported a temperature sensor by doping purely organic Br6A into a PMMA film (Figure 26a).^[94] In addition, polymer tacticity helps to improve the quantum efficiency of the doped system (Figure 26b). Embedding Br6A in isotactic PMMA (iPMMA) results in a relatively high phosphorescence quantum yield of 75%, that is ten times higher compared to Br6A in atactic PMMA (aPMMA) or syndiotactic PMMA (sPMMA) at the same doping level. Moreover, they hypothesized that the quantum yield of the phosphorescence depends on the degree of β-relaxation. Therefore, they explained the tuning of the phosphorescence quantum yield by suppressing the β-relaxation, which should be prone to temperature changes. They then also utilized phosphor G1 doped into a poly(vinyl alcohol) (PVA) matrix (Figure 26c,d), which greatly enhanced the phosphorescence efficiency to 24% by the introduction of

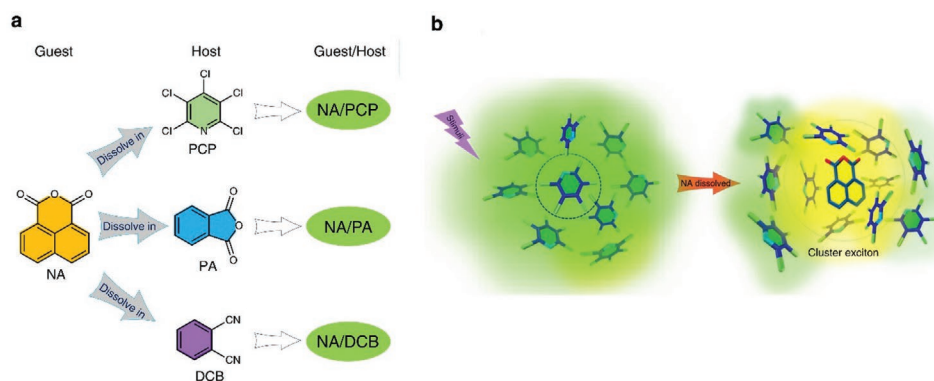


Figure 25. a) Chemical structures of PCP (pentachloropyridine), PA (phthalic anhydride), DCB (1,2-dicyanobenzene), and NA (1,8-naphthalic anhydride). b) Mechanism and application of the guest/host system. Reproduced with permission.^[93] Copyright 2019, Nature Publishing Group.

strong halogen and hydrogen bonds.^[95] Interestingly, when the surface of the G1–PVA film was treated with water, the green phosphorescence transformed into blue fluorescence, which may be useful for ratiometric water sensing. In 2019, Reineke’s group first reported visible-light activated RTP from five hole-transporting materials (Figure 26e) dispersed inside a PMMA film with lifetimes up to 700 ms.^[96] The doped films can be used for printing information through straightforward

erasing/rewriting processes depending on the concentration of oxygen inside the films (Figure 26f). Su’s group developed a simple molecule G, modified by six benzoic acid moieties and select PVA as the polymer matrix (Figure 27a).^[97] Interestingly, G-doped PVA films exhibit RTP lifetimes as long as 0.28 s and quantum efficiencies as high as 2.85%. After irradiation for 65 min with 254 nm light, the corresponding values of τ_p and Φ_p increased to 0.71 s and 11.23%, respectively. They proposed

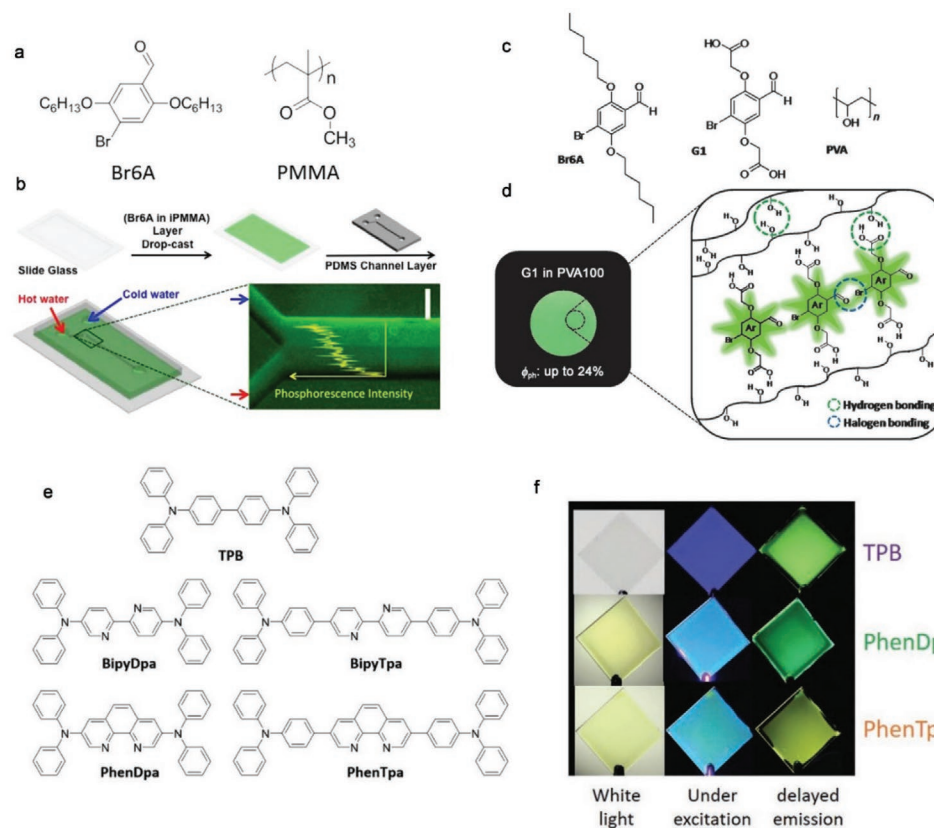


Figure 26. a) Structure of Br6A and PMMA polymer. b) Fabrication method and the microfluidic device prepared from an emitting layer (Br6A in iPMMA) and a PDMS channel layer. Reproduced with permission.^[94] Copyright 2013, American Chemical Society. c) Chemical structures of Br6A, G1, and PVA. d) Phosphorescence image of G1 embedded in PVA100 under UV light ($\lambda = 365$ nm). Reproduced with permission.^[95] Copyright 2014, Wiley-VCH. e) Chemical structures of targeted molecules. f) Photographs of targeted molecules under sunlight (left), under excitation (middle) ($\lambda_{\text{ex}} = 365$ nm for TPB and $\lambda_{\text{ex}} = 420$ nm for PhenDpa and PhenTpa), and after excitation (right). Reproduced with permission.^[96] Copyright 2019, Wiley-VCH.

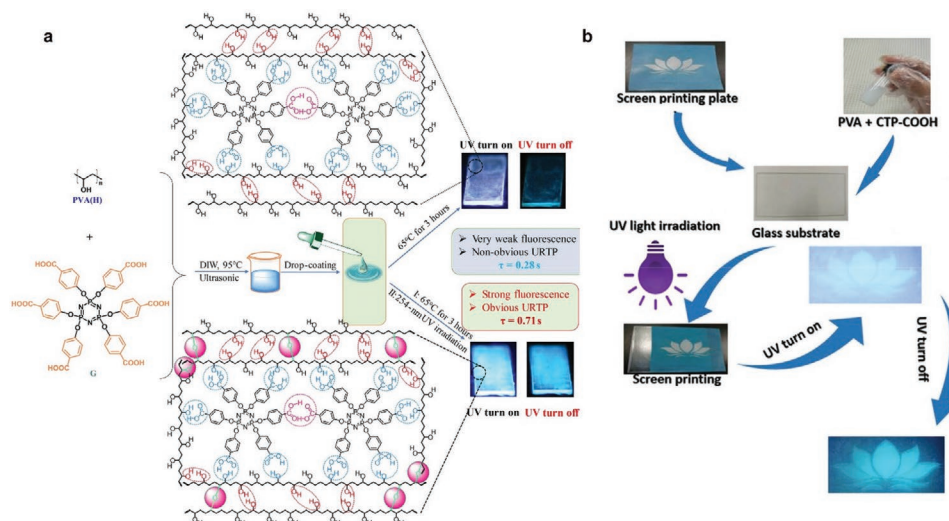


Figure 27. a) Molecular structures of G and PVA and the fabrication method for G-doped PVA films for RTP. b) Green screen printing without any inks using the lotus flower screen plate. Reproduced with permission.^[97] Copyright 2018, Science Publishing Group.

that hydrogen bonds between the PVA matrix and G suppress molecular movement and also boost the ISC process. Under UV light, cross-links formed between PVA chains further reduce nonradiative decay in the films. By changing the irradiation time, they successfully utilized a green screen-printing technology in an anti-counterfeiting application without using any inks (Figure 27b).

4.2.2. RTP from Copolymers

Compared to doping molecules into a polymer matrix, the formation of covalent bonds between polymer and luminophore is a superior way to further restrict nonradiative relaxation pathways because of the more rigid environment. In 2015, Kim et al. reported a diene-modified phosphor (DA1) connected with the polymer PFMA (Figure 28a) by Diels–Alder reaction.^[98] The optimized rigid matrix exhibits persistent RTP with the value of Φ_p up to $\approx 28\%$, which is several times higher than that of the doped system without cross-linking. They also developed an oxygen sensor from core-shell polymer NPs.^[99] They choose polystyrene (PS) as the matrix and water-soluble and biocompatible poly(2-methyl-2-oxazoline) (PMeOx) as the outer shell, connected by a phosphor (Figure 28b). The resulting NPs show an oxygen detection limit of 60 nM which can be applied not only in the gas phase but also in aqueous solution (Figure 28c). In 2020, Zhao and coworkers developed a series of radical cross-linked PDBA (Figure 28e) by multicomponent copolymerization of acrylic acid, vinyl-functionalized naphthalene, and benzene with different molar feed ratio, initiated by 2-azoisobutyronitrile.^[100] Interestingly, when the excitation wavelength is varied from 254 to 370 nm these copolymers show multicolor emissions from blue to yellow (Figure 28d). In addition, the phosphorescent lifetime is up to 1.2 s with a maximum value of Φ_p as high as 37.5% under ambient conditions. They proposed that numerous carbonyl and hydroxyl groups, combined with the tight copolymer environment, not only boost the ISC rate

but also restrict the nonradiative decay of excited triplet state by forming hydrogen bonds. They demonstrated the use of a copolymer for security printing (Figure 28f).

4.2.3. RTP from Molecular Assembly

Self-assembly is also a useful approach to build a rigid molecular framework to suppress nonradiative relaxation for RTP. In 2018, Huang's group designed a multi-component supramolecular system (MA-IPA) containing aromatic acids and melamine (MA) (Figure 29a) in aqueous solution by self-assembly.^[13] The supermolecule constructed shows a persistent lifetime of 1.91 s and Φ_p of 24.3%. Strong hydrogen bonding between isophthalic acid and melamine molecules helps to realize efficient RTP. They successfully printed MA-IPA materials on a piece of filter paper to fabricate a QR code which can be recognized when the UV light was turned off (Figure 29b). Two years later, Ma et al. constructed the self-assembled system TBP-CB[8] by applying a 1:1 ratio of cucurbit[8]uril CB[8] and a triazine derivative TBP, and observed a phosphorescence lifetime of 0.190 ms in aqueous solution (Figure 29c,d).^[101] They proposed that dipole–dipole interactions, hydrophobic interactions, and hydrogen bonding in the stacking patterns of CB[8] and TBP efficiently suppressed the molecular vibrations and rotations. In addition, the photoluminescence emission color of the TBP aqueous solution changes upon continuous addition of CB[8]. According to this phenomenon, they obtained three different hydrogels which show blue, white, and yellow emission when irradiated by 365 nm light (Figure 29e). They also examined bioimaging applications in HeLa cells.

5. RTP from Carbon Dots (CDs)

Because of their low toxicity, chemical stability, and eco-friendly advantages, CDs are used in a variety of applications in

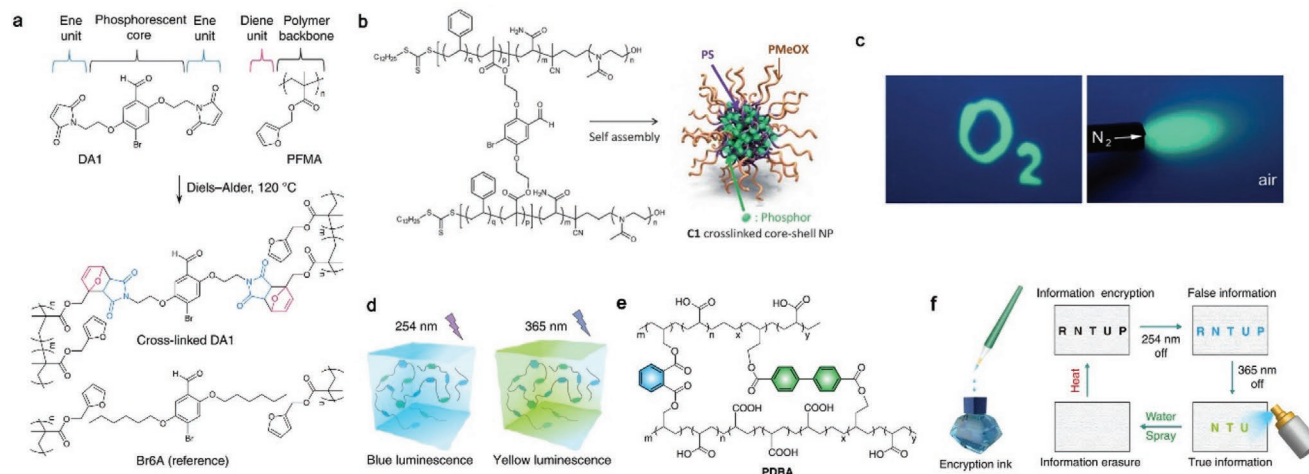


Figure 28. a) Chemical structures of DA1, PFMA, cross-linked DA1, and Br6A. Reproduced with permission.^[98] Copyright 2015, Nature Publishing Group. b) Description of C1-crosslinked NPs. c) Images upon illumination of the planar optical sensor with the 366 nm line of a UV-lamp. Bright green phosphorescence indicates the areas of the sensor soaked with an anoxic aqueous solution for the left image and the area of the sensor deoxygenated with a flow of nitrogen (bottom image). Reproduced with permission.^[99] Copyright 2020, Nature Publishing Group. d) Excitation-dependent RTP ($\lambda_{\text{ex}} = 254$ and 365 nm) of multi-component copolymer under ambient conditions. e) Molecular structure of polymer PDNA. f) Process of information encryption by using the multi-component copolymer PDNA (NTU) and PDA (RP) as encryption ink under ambient conditions. Reproduced with permission.^[100] Copyright 2017, Wiley-VCH.

bioimaging, LEDs, and sensors. However, most research treats CDs as fluorescent nanomaterials, and seldom were their RTP properties considered for applications. In 2016, Yang's group mixed N-doped CDs (NCDs) with melting recrystallization urea and biuret matrices through a one-pot process.^[102] The multi-component matrices provide efficient hydrogen bonding and a rigid environment to suppress nonradiative decay (Figure 30a). More importantly, they proposed that C=N double bonds at the surface of NCDs could decrease the ΔE_{ST} and boost electronic transitions by creating new energy levels. In 2018, Lin et al. first introduced RTP polymer CDs (Figure 30b) through heating ethylenediamine and phosphoric acid.^[103] The green afterglow can remain for almost 10 s and the phosphorescence lifetime is up to 1.39 s (Figure 30c). Heating ethylenediamine and phosphoric acid at 180 °C formed only fluorescent CDs. Upon increasing the temperature to 280 °C, further crosslinking reactions in the F-CDs occurred, resulting in

more compact P-CDs. On one hand, the denser structure could effectively restrict vibrations and rotations. On the other hand, the N- and P-doping elements bearing lone pairs provided $n \rightarrow \pi^*$ transitions to populate triplet states and thus accelerate the rate of ISC. Two years later, in 2020, they also developed TA-CDs (Figure 30d) with aggregation-induced RTP properties.^[104] Interestingly, they successfully applied TA-CD dispersions as an anti-counterfeiting agent and, in addition, the RTP is responsive to moisture (Figure 30e). Shi et al. also reported persistent RTP from CDs induced by the presence of water.^[105] They proposed that water could build robust networks between CDs and cyanuric acid (CA) via hydrogen bonds (Figure 30f). The rigid matrix effectively restricts molecular movement and thus reduces nonradiative decay, resulting in a long phosphorescence lifetime (687 ms). Moreover, multiple C=O bonds in the entire CD-CA system increase transitions of $n \rightarrow \pi^*$ type and greatly enhance the ISC process. They also applied CD-CA

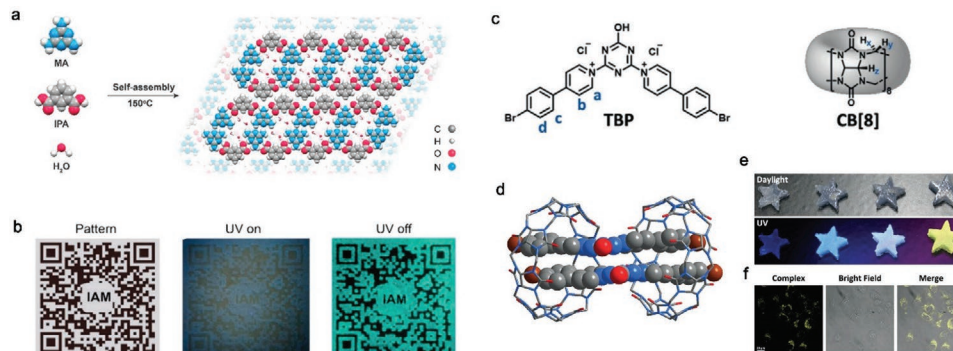


Figure 29. a) Design concept of supramolecular architecture. b) Application of ultralong phosphors in a QR code. Reproduced with permission.^[13] Copyright 2018, American Chemical Society. c) Structures of CB[8] and TBP. d) Side view of crystalline structure of the (TBP)₂-CB[8]₂ assembly. C, gray; N, blue; O, red; Br, brown. e) Pictures of multicolor hydrogels irradiated by sunlight and 365 nm light. f) Luminescent images of HeLa cells treated with TBP-CB[8] complex (left), bright field (middle), and merge (right) confocal. Reproduced with permission.^[101] Copyright 2020, Wiley-VCH.

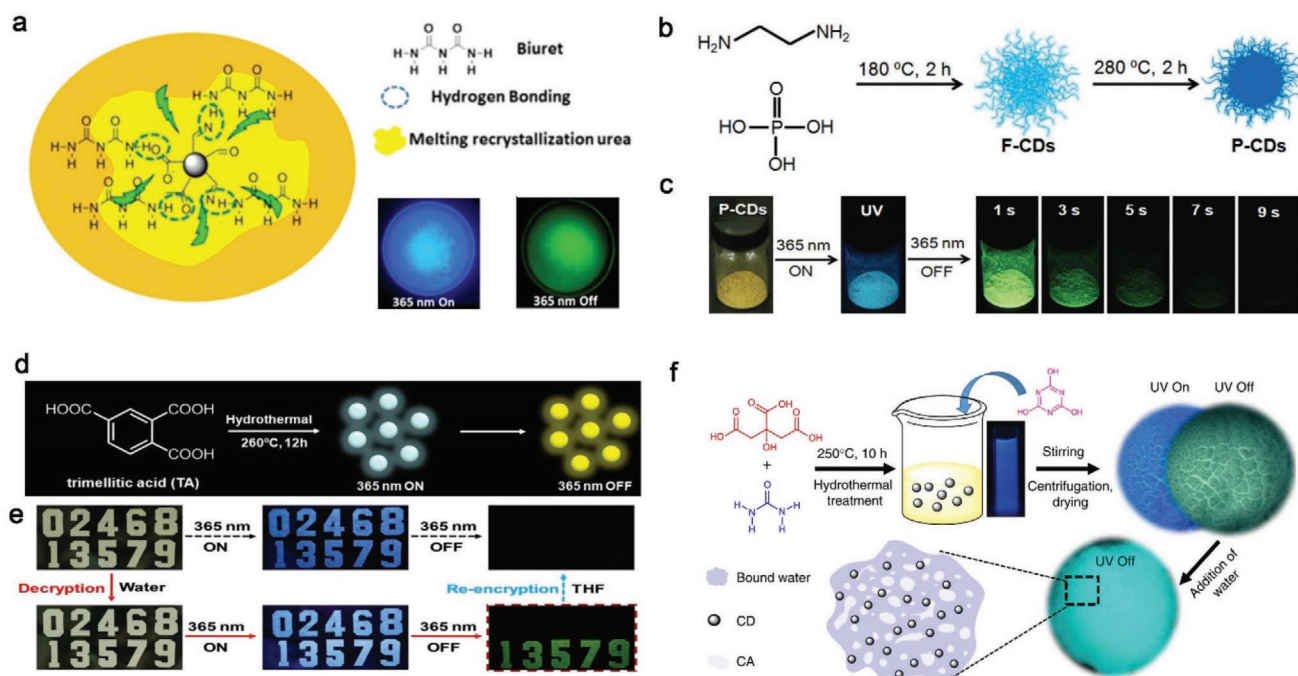


Figure 30. a) NCDs are inserted into urea and biuret matrices. Reproduced with permission.^[101] Copyright 2016, American Chemical Society. b) Procedures for the preparation of F-CDs and P-CDs. c) Afterglow images of the P-CD powder. Reproduced with permission.^[102] Copyright 2018, Wiley-VCH. d) The synthetic method for preparing TA-CDs, and RTP photographs irradiated by UV light. e) Information encryption and decryption processes using TA-CDs and interference CDs inks. Reproduced with permission.^[104] Copyright 2020, Wiley-VCH. f) Preparation method for the CDs and the CD-CA system. Reproduced with permission.^[105] Copyright 2018, Nature Publishing Group.

suspensions to detect Fe^{3+} ions in water. The phosphorescence intensity gradually decreased with the addition of Fe^{3+} ions. This method, based on phosphorescence quenching, has a detection limit of $32 \mu\text{M}$ for Fe^{3+} , making it a good candidate for ion sensor applications. In 2019, Rogach et al. developed color-tunable powdered CDs with RTP properties by controlling CD growth (Figure 31a).^[15] The RTP phenomenon is enhanced by a variety of nitrogen-containing moieties on the surface, such as $-\text{NH}_2$, $\text{C}=\text{N}$, and $\text{C}-\text{N}$ bonds (Figure 31b). In addition, the polyvinylpyrrolidone polymer chains protect the CDs from coming into contact with quenching species, therefore, preventing nonradiative pathways, especially in a CD-5.6 powder with large NPs (Figure 31c). Finally, they also showed an example of the utilization of CD-5.6 for data encryption.

6. Outlook

In order to achieve persistent RTP materials, much effort has been devoted to diversified molecular design in both single-molecule and multi-component systems. Intense study has shown that heteroatoms (N, O, and S) or corresponding functional groups are especially useful in realizing efficient RTP.^[106] Therefore, carbazole,^[107] indoline,^[108] quinoline,^[109] phenothiazine,^[110] and their derivatives^[111] account for the majority of RTP luminophores. The reason is simple: these atoms and related moieties bear lone pairs which enhance the rate of the ISC process through El-Sayed's rule.^[112] In addition, the active

sites in these molecules make it easy to fabricate the desired phosphors and the total cost is quite low. We also point out that 3-coordinate boron, with an empty p_z orbital, can also

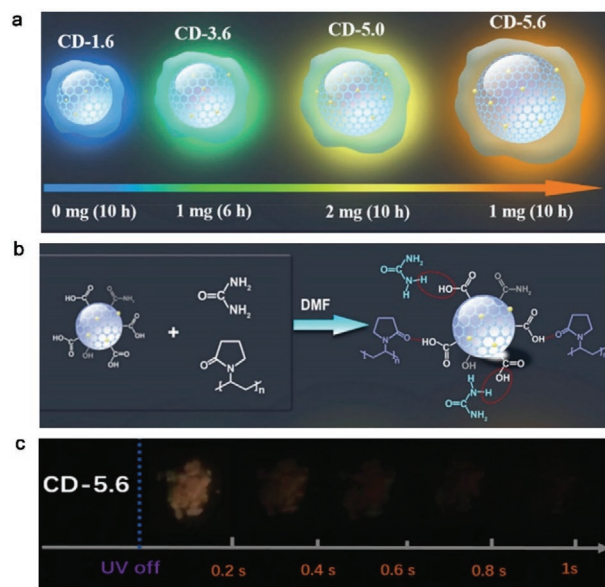


Figure 31. a) Four different CD sizes. b) Seeded growth reaction for formation of CDs. c) Afterglow images of the CD-5.6 powders under irradiation at 365 nm. Reproduced with permission.^[15] Copyright 2019, Wiley-VCH.

accelerate ISC processes via transitions between (σ , B p) and (π , B p), indicating that introducing lone pairs is only one way to enhance ISC.^[22] This new finding makes boron-containing compounds, especially triarylboranes, good candidates for RTP luminophores. Considering the development of efficient RTP materials in the future, a systematic study of existing systems is essential to help us clearly elucidate the mechanism behind these photoluminescent properties. However, the types of RTP systems with high performance are still quite limited. The discovery of new persistent RTP systems is always inspiring and will also expand our insight into the origin of purely organic phosphorescent phenomena.

The main issue is to enhance the RTP lifetime and efficiency at the same time. Based on our current understanding, there are mainly two strategies to achieve this aim. One is to populate the triplet state by speeding up the ISC process. What we address here are commonly used heavy atoms which can enhance SOC. From the perspective of cost and environmental issues, the synthetic expense of RTP luminophores with heavy atoms is higher and they are not as environmentally friendly. In addition, it is hard to achieve a balance between phosphorescence lifetime and quantum yield, as introducing heavy atoms also boosts radiative decay rates from the triplet state, which shortens the lifetime; therefore, the trend is to omit heavy atoms in the design of RTP systems. Another strategy is to restrict the non-radiative pathways, as RTP performance not only relies on molecular structure but also depends on the aggregation state. Crystallization methods play a major role in suppressing non-radiative decay, which requires rigid packing modes and strong intermolecular interactions in the crystalline matrix.^[113] To achieve an ideal crystalline environment with efficient RTP is quite challenging and currently unpredictable through rational molecular design. It also limits practical use if high performance of RTP is only possible in the crystalline state. At the same time, it is crucial to reduce the trap concentration in a crystal which is an important factor for triplet quenching, which can be achieved by using crystals of the highest purity.^[44] As an alternative, amorphous RTP materials such as polymers,^[114] are more competitive due to their easier processibility and high environmental stability, although the intrinsic mechanism still needs systematic study and further exploration. Another approach is to develop host-guest systems which do not require a strict crystalline environment. More importantly, this enables otherwise non-emissive luminophores to emit strong and persistent RTP under ambient conditions, which greatly enlarges the variety of RTP phosphors. Host-guest systems are quite promising, but the underlying driving force needs further clarification for rational design.

Because of their superior lifetimes, RTP materials are widely used in security printing and bioimaging fields.^[115] Compared to fluorescence, phosphorescence enabling long afterglow which cannot be replicated by fluorescent dyes, and is helpful to remove short-lived background emissions.^[109] In order to realize anti-counterfeiting applications of RTP materials in real life, more effort should be put into industrial development and commercialization. For future developments in bioimaging, it is vital to explore red and NIR RTP phosphors because red light emission provides deeper tissue penetration and less photon

scattering. Due to their bright phosphorescence, RTP phosphors have also been applied in OLEDs.^[105] Although intense work was conducted on PHOLEDs, deep blue and white light devices based on RTP materials are still a challenge. So far, there have been fewer applications in sensing compared to other fields. It is necessary to find new candidates and to improve detection limits at the same, for practical use.

Recently, many concerns have been raised regarding impurities in purely organic RTP materials, especially in carbazole-based phosphors. We stress that much work has already proven that confirmed pure carbazole-based luminophores show persistent RTP phenomenon. However, it is necessary to re-examine some of the previously reported examples, as trace impurities greatly influence their photophysical properties. For future work, we suggest that, in purely organic RTP systems, it is critical to re-examine their photophysical properties after further purifications of the sample, such as multiple recrystallizations. While it may not be possible to remove the impurity completely by normal purification methods, its reduction in the sample should result in obvious changes in phosphorescence emission, lifetime and quantum yield. The varying results induced by different amounts of impurities are already indicated in many reports, make this purification step necessary for reliable results.

7. Conclusions

Benefiting from the high degree of structural diversity of organic molecules, a variety of room-temperature phosphors have been designed and synthesized in the last two decades. Their applications in oxygen sensors, security printing, and biological imaging have been widely tested. There are mainly two basic approaches to achieving efficient RTP. The first is to focus on enhancing ISC as Equations (2) and (3) indicate that phosphorescence largely depends on the rate of the ISC process. Therefore, elements bearing lone pairs (N, O, S) or their corresponding functional groups are utilized for the realization of room-temperature phosphors. The second strategy is to reduce the nonradiative decay rate of the triplet state(s) which has a direct effect on the efficiency of phosphorescence. A popular method is to dope luminophores into a polymer matrix or to construct host-guest systems. More recently, the introduction of CDs has received much attention due to their advantages, such as easy modification and chemical stability. However, it is still difficult to develop a universal and systematic method to predict and prepare RTP materials. In order to broaden the range of practical applications of organic RTP materials, the mechanism of phosphorescent emission needs to be explored further. Moreover, developing high-performance RTP materials bearing excellent values of τ_p and Φ_p simultaneously remains a formidable challenge as they are mutually influenced. However, new breakthroughs can be expected and new types of organic RTP materials are likely to result. Finally, we note again that extreme care must be taken to assure the purity of all compounds employed, as even trace impurities can give rise to anomalous results. Thus, some of the systems which have been reported probably warrant re-examination by other researchers.

Acknowledgements

Support from the Julius-Maximilians-Universität Würzburg is gratefully acknowledged. Z.W. thanks the China Scholarship Council for a Ph.D. scholarship.

Open access funding enabled and organized by Projekt DEAL.

Conflict of Interest

The authors declare no conflict of interest.

Keywords

intersystem crossing, luminescence, non-radiative decay, photophysics, polymer matrix

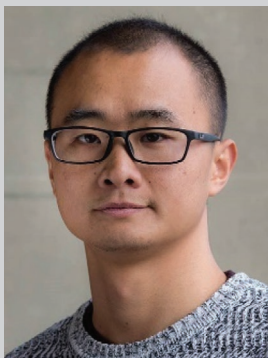
Received: February 25, 2021

Revised: June 3, 2021

Published online: July 3, 2021

- [1] H. Chen, X. Yao, X. Ma, H. Tian, *Adv. Opt. Mater.* **2016**, *4*, 1397.
- [2] S. Reineke, F. Lindner, G. Schwartz, N. Seidler, K. Walzer, B. Lussem, K. Leo, *Nature* **2009**, *459*, 234.
- [3] A. Kishimura, T. Yamashita, K. Yamaguchi, T. Aida, *Nat. Mater.* **2005**, *4*, 546.
- [4] L. Huang, C. Qian, Z. Ma, *Chem. - Eur. J.* **2020**, *26*, 11914.
- [5] S. Xu, R. Chen, C. Zheng, W. Huang, *Adv. Mater.* **2016**, *28*, 9920.
- [6] J. Zhao, W. Wu, J. Sun, S. Guo, *Chem. Soc. Rev.* **2013**, *42*, 5323.
- [7] S. Mukherjee, P. Thilagar, *Chem. Commun.* **2015**, *51*, 10988.
- [8] X. Ma, J. Wang, H. Tian, *Acc. Chem. Res.* **2019**, *52*, 738.
- [9] T. Zhang, X. Ma, H. Wu, L. Zhu, Y. Zhao, H. Tian, *Angew. Chem., Int. Ed.* **2020**, *59*, 11206.
- [10] J. Wang, C. Wang, Y. Gong, Q. Liao, M. Han, T. Jiang, Q. Dang, Y. Li, Q. Li, Z. Li, *Angew. Chem., Int. Ed.* **2018**, *57*, 16821.
- [11] E. Hamzehpoor, D. F. Perepichka, *Angew. Chem., Int. Ed.* **2020**, *59*, 9977.
- [12] T. Wang, C. Zhou, X. Zhang, D. Xu, *Polym. Chem.* **2018**, *9*, 1303.
- [13] L. Bian, H. Shi, X. Wang, K. Ling, H. Ma, M. Li, Z. Cheng, C. Ma, S. Cai, Q. Wu, N. Gan, X. Xu, Z. An, W. Huang, *J. Am. Chem. Soc.* **2018**, *140*, 10734.
- [14] T. Ono, A. Taema, A. Goto, Y. Hisaeda, *Chem. - Eur. J.* **2018**, *24*, 17487.
- [15] J. Zhu, X. Bai, X. Chen, H. Shao, Y. Zhai, G. Pan, H. Zhang, E. V. Ushakova, Y. Zhang, H. Song, A. L. Rogach, *Adv. Opt. Mater.* **2019**, *7*, 1801599.
- [16] T. J. Penfold, E. Gindensperger, C. Daniel, C. M. Marian, *Chem. Rev.* **2018**, *118*, 6975.
- [17] H. Matsuoka, M. Retegan, L. Schmitt, S. Hoyer, F. Neese, O. Schiemann, *J. Am. Chem. Soc.* **2017**, *139*, 12968.
- [18] J. S. Ward, R. S. Nobuyasu, M. A. Fox, A. S. Batsanov, J. Santos, F. B. Dias, M. R. Bryce, *J. Org. Chem.* **2018**, *83*, 14431.
- [19] R. Joshi, O. R. Meitei, M. Jadhao, H. Kumar, S. K. Ghosh, *Phys. Chem. Chem. Phys.* **2016**, *18*, 27910.
- [20] S. Kuno, T. Kanamori, Z. Yijing, H. Ohtani, H. Yuasa, *ChemPhotoChem* **2017**, *1*, 102.
- [21] J. Yang, Z. Ren, Z. Xie, Y. Liu, C. Wang, Y. Xie, Q. Peng, B. Xu, W. Tian, F. Zhang, Z. Chi, Q. Li, Z. Li, *Angew. Chem., Int. Ed.* **2017**, *56*, 880.
- [22] Z. Wu, J. Nitsch, J. Schuster, A. Friedrich, K. Edkins, M. Loebnitz, F. Dinkelbach, V. Stepanenko, F. Würthner, C. M. Marian, L. Ji, T. B. Marder, *Angew. Chem., Int. Ed.* **2020**, *59*, 17137.
- [23] C. A. M. Salla, G. Farias, M. Rouzieres, P. Dechambenoit, F. Durola, H. Bock, B. de Souza, I. H. Bechtold, *Angew. Chem., Int. Ed.* **2019**, *58*, 6982.
- [24] H. Yuasa, S. Kuno, *Bull. Chem. Soc. Jpn.* **2018**, *91*, 223.
- [25] C. Chen, Z. Chi, K. C. Chong, A. S. Batsanov, Z. Yang, Z. Mao, Z. Yang, B. Liu, *Nat. Mater.* **2020**, *20*, 175.
- [26] H. T. Feng, J. Zeng, P. A. Yin, X. D. Wang, Q. Peng, Z. Zhao, J. W. Y. Lam, B. Z. Tang, *Nat. Commun.* **2020**, *11*, 2617.
- [27] H. Li, H. Li, W. Wang, Y. Tao, S. Wang, Q. Yang, Y. Jiang, C. Zheng, W. Huang, R. Chen, *Angew. Chem. Int. Ed.* **2020**, *59*, 4756.
- [28] Z. An, C. Zheng, Y. Tao, R. Chen, H. Shi, T. Chen, Z. Wang, H. Li, R. Deng, X. Liu, W. Huang, *Nat. Mater.* **2015**, *14*, 685.
- [29] Y. Gong, G. Chen, Q. Peng, W. Z. Yuan, Y. Xie, S. Li, Y. Zhang, B. Z. Tang, *Adv. Mater.* **2015**, *27*, 6195.
- [30] C. Li, X. Tang, L. Zhang, C. Li, Z. Liu, Z. Bo, Y. Q. Dong, Y.-H. Tian, Y. Dong, B. Z. Tang, *Adv. Opt. Mater.* **2015**, *3*, 1184.
- [31] Z. Mao, Z. Yang, Y. Mu, Y. Zhang, Y. F. Wang, Z. Chi, C. C. Lo, S. Liu, A. Lien, J. Xu, *Angew. Chem., Int. Ed.* **2015**, *54*, 6270.
- [32] P. Xue, J. Sun, P. Chen, P. Wang, B. Yao, P. Gong, Z. Zhang, R. Lu, *Chem. Commun.* **2015**, *51*, 10381.
- [33] Z. Yang, Z. Mao, X. Zhang, D. Ou, Y. Mu, Y. Zhang, C. Zhao, S. Liu, Z. Chi, J. Xu, Y. C. Wu, P. Y. Lu, A. Lien, M. R. Bryce, *Angew. Chem., Int. Ed.* **2016**, *55*, 2181.
- [34] S. Cai, H. Shi, J. Li, L. Gu, Y. Ni, Z. Cheng, S. Wang, W. W. Xiong, L. Li, Z. An, W. Huang, *Adv. Mater.* **2017**, *29*, 1701244.
- [35] S. M. A. Fateminia, Z. Mao, S. Xu, Z. Yang, Z. Chi, B. Liu, *Angew. Chem., Int. Ed.* **2017**, *56*, 12160.
- [36] Y. Xie, Y. Ge, Q. Peng, C. Li, Q. Li, Z. Li, *Adv. Mater.* **2017**, *29*, 1606829.
- [37] S. Cai, H. Shi, Z. Zhang, X. Wang, H. Ma, N. Gan, Q. Wu, Z. Cheng, K. Ling, M. Gu, C. Ma, L. Gu, Z. An, W. Huang, *Angew. Chem., Int. Ed.* **2018**, *57*, 4005.
- [38] Y. Tao, R. Chen, H. Li, J. Yuan, Y. Wan, H. Jiang, C. Chen, Y. Si, C. Zheng, B. Yang, G. Xing, W. Huang, *Adv. Mater.* **2018**, *30*, 1803856.
- [39] Y. Xiong, Z. Zhao, W. J. Zhao, H. L. Ma, Q. Peng, Z. K. He, X. P. Zhang, Y. C. Chen, X. W. He, J. Lam, B. Z. Tang, *Angew. Chem., Int. Ed.* **2018**, *27*, 8129.
- [40] L. Xu, G. Li, T. Xu, W. Zhang, S. Zhang, S. Yin, Z. An, G. He, *Chem. Commun.* **2018**, *54*, 9226.
- [41] Z. He, H. Gao, S. Zhang, S. Zheng, Y. Wang, Z. Zhao, D. Ding, B. Yang, Y. Zhang, W. Z. Yuan, *Adv. Mater.* **2019**, *31*, 1807222.
- [42] L. Huang, L. Liu, X. Li, H. Hu, M. Chen, Q. Yang, Z. Ma, X. Jia, *Angew. Chem., Int. Ed.* **2019**, *58*, 16445.
- [43] X. Liang, T. T. Liu, Z. P. Yan, Y. Zhou, J. Su, X. F. Luo, Z. G. Wu, Y. Wang, Y. X. Zheng, J. L. Zuo, *Angew. Chem., Int. Ed.* **2019**, *58*, 17220.
- [44] A. D. Nidhankar, V. C. W. Goudappagouda, S. S. Babu, *Chem. Sci.* **2021**, *12*, 4216.
- [45] S. Hirata, *Adv. Opt. Mater.* **2017**, *5*, 1700116.
- [46] M. Baroncini, G. Bergamini, P. Ceroni, *Chem. Commun.* **2017**, *53*, 2081.
- [47] A. P. Demchenko, V. I. Tomin, P. T. Chou, *Chem. Rev.* **2017**, *117*, 13353.
- [48] S. Hirata, *J. Mater. Chem. C* **2018**, *6*, 11785.
- [49] A. Forni, E. Lucenti, C. Botta, E. Cariati, *J. Mater. Chem. C* **2018**, *6*, 4603.
- [50] J. A. Li, J. Zhou, Z. Mao, Z. Xie, Z. Yang, B. Xu, C. Liu, X. Chen, D. Ren, H. Pan, G. Shi, Y. Zhang, Z. Chi, *Angew. Chem., Int. Ed.* **2018**, *57*, 6449.
- [51] Goudappagouda, A. Manthanath, V. C. Wakchaure, Kayaramkodath, C. Ranjeesh, T. Das, K. Vanka, T. Nakanishi, S. S. Babu, *Angew. Chem., Int. Ed.* **2018**, *131*, 2306.
- [52] D. Wang, Z. Yan, M. Shi, J. Dai, Q. Chai, H. Gui, Y. Zhang, X. Ma, *Adv. Opt. Mater.* **2019**, *7*, 1901277.

- [53] W. Liu, J. Wang, Y. Gong, Q. Liao, Q. Dang, Z. Li, Z. Bo, *Angew. Chem., Int. Ed.* **2020**, *132*, 20336.
- [54] Z. Chai, C. Wang, J. Wang, F. Liu, Y. Xie, Y.-Z. Zhang, J.-R. Li, Q. Li, Z. Li, *Chem. Sci.* **2017**, *8*, 8336.
- [55] M. Li, X. Cai, Z. Qiao, K. Liu, W. Xie, L. Wang, N. Zheng, S. J. Su, *Chem. Commun.* **2019**, *55*, 7215.
- [56] Y. Shoji, Y. Ikabata, Q. Wang, D. Nemoto, A. Sakamoto, N. Tanaka, J. Seino, H. Nakai, T. Fukushima, *J. Am. Chem. Soc.* **2017**, *139*, 2728.
- [57] Y. Zhou, W. Qin, C. Du, H. Gao, F. Zhu, G. Liang, *Angew. Chem., Int. Ed.* **2019**, *58*, 12102.
- [58] M. Ferger, S. M. Berger, F. Rauch, S. Schönitz, J. Rühle, J. Krebs, A. Friedrich, T. B. Marder, *Chem. - Eur. J.* **2021**, *27*, 9094.
- [59] S. M. Berger, M. Ferger, T. B. Marder, *Chem. - Eur. J.* **2021**, *27*, 7043.
- [60] J.-L. Ma, H. Liu, S.-Y. Li, Z.-Y. Li, H.-Y. Zhang, Y. Wang, C.-H. Zhao, *Organometallics* **2020**, *39*, 4153.
- [61] G. Q. Zhang, J. B. Chen, S. J. Payne, S. E. Kooi, J. N. Demas, C. L. Fraser, *J. Am. Chem. Soc.* **2007**, *129*, 8942.
- [62] G. Zhang, G. M. Palmer, M. W. Dewhurst, C. L. Fraser, *Nat. Mater.* **2009**, *8*, 747.
- [63] Z. Yu, Y. Wu, L. Xiao, J. Chen, Q. Liao, J. Yao, H. Fu, *J. Am. Chem. Soc.* **2017**, *139*, 6376.
- [64] Z. Xu, Q. T. Liu, X. Z. Wang, Q. Liu, D. Hean, K. C. Chou, M. O. Wolf, *Chem. Sci.* **2020**, *11*, 2729.
- [65] J. S. Ward, R. S. Nobuyasu, A. S. Batsanov, P. Data, A. P. Monkman, F. B. Dias, M. R. Bryce, *Chem. Commun.* **2016**, *52*, 2612.
- [66] J. S. Ward, R. S. Nobuyasu, M. A. Fox, J. A. Aguilar, D. Hall, A. S. Batsanov, Z. Ren, F. B. Dias, M. R. Bryce, *J. Org. Chem.* **2019**, *84*, 3801.
- [67] J. Yang, X. Zhen, B. Wang, X. Gao, Z. Ren, J. Wang, Y. Xie, J. Li, Q. Peng, K. Pu, Z. Li, *Nat. Commun.* **2018**, *9*, 840.
- [68] J. Yang, H. Gao, Y. Wang, Y. Yu, Y. Gong, M. Fang, D. Ding, W. Hu, B. Z. Tang, Z. Li, *Mater. Chem. Front.* **2019**, *3*, 1391.
- [69] L. K. Huang, B. Chen, X. P. Zhang, C. O. Trindle, F. Liao, Y. C. Wang, H. Miao, Y. Luo, G. Q. Zhang, *Angew. Chem., Int. Ed.* **2018**, *57*, 16046.
- [70] Z. Y. Liu, J. W. Hu, C. H. Huang, T. H. Huang, D. G. Chen, S. Y. Ho, K. Y. Chen, E. Y. Li, P. T. Chou, *J. Am. Chem. Soc.* **2019**, *141*, 9885.
- [71] L. Yu, Z. Wu, C. Zhong, G. Xie, Z. Zhu, D. Ma, C. Yang, *Adv. Opt. Mater.* **2017**, *5*, 1700588.
- [72] C. Zhou, S. Zhang, Y. Gao, H. Liu, T. Shan, X. Liang, B. Yang, Y. Ma, *Adv. Funct. Mater.* **2018**, *28*, 1802407.
- [73] M. Shimizu, R. Shigitani, M. Nakatani, K. Kuwabara, Y. Miyake, K. Tajima, H. Sakai, T. Hasobe, *J. Phys. Chem. C* **2016**, *120*, 11631.
- [74] M. Shimizu, T. Kinoshita, R. Shigitani, Y. Miyake, K. Tajima, *Mater. Chem. Front.* **2018**, *2*, 347.
- [75] Q. Li, Z. Li, *Acc. Chem. Res.* **2020**, *53*, 962.
- [76] A. D. Nidhankar, D. S. M. K. Goudappagouda, S. K. Chaubey, R. Nayak, R. G. Gonnade, G. V. P. Kumar, R. Krishnan, S. S. Babu, *Angew. Chem., Int. Ed.* **2020**, *59*, 13079.
- [77] Z. Ruan, Q. Liao, Q. Dang, X. Chen, C. Deng, Z. Gao, J. Lin, S. Liu, Y. Chen, Z. Tian, Z. Li, *Adv. Opt. Mater.* **2021**, *9*, 2001549.
- [78] X. F. Wang, H. Y. Xiao, P. Z. Chen, Q. Z. Yang, B. Chen, C. H. Tung, Y. Z. Chen, L. Z. Wu, *J. Am. Chem. Soc.* **2019**, *141*, 5045.
- [79] J. Wang, X. Gu, H. Ma, Q. Peng, X. Huang, X. Zheng, S. H. P. Sung, G. Shan, J. W. Y. Lam, Z. Shuai, B. Z. Tang, *Nat. Commun.* **2018**, *9*, 2963.
- [80] F. Li, S. Guo, Y. Qin, Y. Shi, M. Han, Z. An, S. Liu, Q. Zhao, W. Huang, *Adv. Opt. Mater.* **2019**, *7*, 1900511.
- [81] R. Kabe, C. Adachi, *Nature* **2017**, *550*, 384.
- [82] Z. Lin, R. Kabe, K. Wang, C. Adachi, *Nat. Commun.* **2020**, *11*, 191.
- [83] B. B. Ding, L. W. Ma, Z. Z. Huang, X. Ma, H. Tian, *ChemRxiv* **2021**, <https://doi.org/10.26434/chemrxiv.13285589.v1>.
- [84] B. Chen, W. Huang, H. Su, H. Miao, X. Zhang, G. Zhang, *Angew. Chem., Int. Ed.* **2020**, *59*, 10023.
- [85] O. Bolton, K. Lee, H. J. Kim, K. Y. Lin, J. Kim, *Nat. Chem.* **2011**, *3*, 205.
- [86] O. Bolton, D. Lee, J. Jung, J. Kim, *Chem. Mater.* **2014**, *26*, 6644.
- [87] S. Hirata, K. Totani, J. Zhang, T. Yamashita, H. Kaji, S. R. Marder, T. Watanabe, C. Adachi, *Adv. Funct. Mater.* **2013**, *23*, 3386.
- [88] S. Hirata, K. Totani, H. Kaji, M. Vacha, T. Watanabe, C. Adachi, *Adv. Opt. Mater.* **2013**, *1*, 438.
- [89] R. Kabe, N. Notsuka, K. Yoshida, C. Adachi, *Adv. Mater.* **2016**, *28*, 655.
- [90] J. Wei, B. Liang, R. Duan, Z. Cheng, C. Li, T. Zhou, Y. Yi, Y. Wang, *Angew. Chem., Int. Ed.* **2016**, *55*, 15589.
- [91] L. Xiao, Y. Wu, Z. Yu, Z. Xu, J. Li, Y. Liu, J. Yao, H. Fu, *Chem. - Eur. J.* **2018**, *24*, 1801.
- [92] D. Li, F. Lu, J. Wang, W. Hu, X. M. Cao, X. Ma, H. Tian, *J. Am. Chem. Soc.* **2018**, *140*, 1916.
- [93] X. Zhang, L. Du, W. Zhao, Z. Zhao, Y. Xiong, X. He, P. F. Gao, P. Alam, C. Wang, Z. Li, J. Leng, J. Liu, C. Zhou, J. W. Y. Lam, D. L. Phillips, G. Zhang, B. Z. Tang, *Nat. Commun.* **2019**, *10*, 5161.
- [94] D. Lee, O. Bolton, B. C. Kim, J. H. Youk, S. Takayama, J. Kim, *J. Am. Chem. Soc.* **2013**, *135*, 6325.
- [95] M. S. Kwon, D. Lee, S. Seo, J. Jung, J. Kim, *Angew. Chem., Int. Ed.* **2014**, *53*, 11177.
- [96] M. Louis, H. Thomas, M. Gmelch, A. Haft, F. Fries, S. Reineke, *Adv. Mater.* **2019**, *31*, 1807887.
- [97] Y. Su, S. Z. F. Phua, Y. B. Li, X. J. Zhou, D. B. Jana, G. F. Liu, W. Q. Lim, W. K. Ong, C. L. Yang, Y. Zhao, *Sci. Adv.* **2018**, *4*, eaas9732.
- [98] M. S. Kwon, Y. Yu, C. Coburn, A. W. Phillips, K. Chung, A. Shanker, J. Jung, G. Kim, K. Pipe, S. R. Forrest, J. H. Youk, J. Gierschner, J. Kim, *Nat. Commun.* **2015**, *6*, 8947.
- [99] Y. Yu, M. S. Kwon, J. Jung, Y. Zeng, M. Kim, K. Chung, J. Gierschner, J. H. Youk, S. M. Borisov, J. Kim, *Angew. Chem., Int. Ed.* **2017**, *56*, 16207.
- [100] L. Gu, H. Wu, H. Ma, W. Ye, W. Jia, H. Wang, H. Chen, N. Zhang, D. Wang, C. Qian, Z. An, W. Huang, Y. Zhao, *Nat. Commun.* **2020**, *11*, 944.
- [101] J. Wang, Z. Huang, X. Ma, H. Tian, *Angew. Chem., Int. Ed.* **2020**, *59*, 9928.
- [102] Q. Li, M. Zhou, Q. Yang, Q. Wu, J. Shi, A. Gong, M. Yang, *Chem. Mater.* **2016**, *28*, 8221.
- [103] K. Jiang, Y. Wang, C. Cai, H. Lin, *Adv. Mater.* **2018**, *30*, 1800783.
- [104] K. Jiang, X. Gao, X. Feng, Y. Wang, Z. Li, H. Lin, *Angew. Chem., Int. Ed.* **2020**, *59*, 1263.
- [105] Q. Li, M. Zhou, M. Yang, Q. Yang, Z. Zhang, J. Shi, *Nat. Commun.* **2018**, *9*, 734.
- [106] W. Zhao, Z. He, B. Z. Tang, *Nat. Rev. Mater.* **2020**, *5*, 869.
- [107] Q. Peng, H. Ma, Z. Shuai, *Acc. Chem. Res.* **2021**, *54*, 940.
- [108] M. Singh, K. Liu, S. Qu, H. Ma, H. Shi, Z. An, W. Huang, *Adv. Opt. Mater.* **2021**, *9*, 2002197.
- [109] L. Xiao, H. Fu, *Chem. - Eur. J.* **2019**, *25*, 714.
- [110] C. C. Kenry, B. Liu, *Nat. Commun.* **2019**, *10*, 2111.
- [111] M.-M. Fang, J. Yang, Z. Li, *Chin. J. Polym. Sci.* **2019**, *37*, 383.
- [112] J. Yang, Z. Chi, W. Zhu, B. Z. Tang, Z. Li, *Sci. China: Chem.* **2019**, *62*, 1090.
- [113] J. Gierschner, J. Q. Shi, B. M. Medina, D. R. Sanjuán, S. Varghese, S. Y. Park, *Adv. Opt. Mater.* **2021**, 2002251.
- [114] G. Qu, Y. Zhang, X. Ma, *Chin. Chem. Lett.* **2019**, *30*, 1809.
- [115] H. Tian, X. Ma, C. Xu, J. Wang, *Angew. Chem., Int. Ed.* **2018**, *57*, 10854.



Zhu Wu received his bachelor's degree from Soochow University, China, in 2014. He obtained his master's degree from Jilin University, China, in 2017. Then he joined Prof. Marder's group at the University of Würzburg for his Ph.D. He is currently carrying out research on RTP from triarylborane chromophores. In addition, he has also worked on radical anions and dianions formed from the reductions of tetraazapentacenes and their derivatives.



Jörn Nitsch obtained his diploma from WWU Münster and his Ph.D. from the University of Würzburg in 2015, where he worked on the development of novel luminescent copper (I) complexes for OLEDs. After a two-year DFG postdoctoral fellowship with Prof. F. Matthias Bickelhaupt in Amsterdam, focusing on theoretical chemistry and working on the description of excited states, he joined Prof. Todd B. Marder's research group in 2018. Besides RTP materials, his research is focused on the development of new TADF emitters for OLEDs and other light-emitting devices, and the modeling of excited states in luminescent compounds.



Todd B. Marder obtained his B.Sc. from MIT and his Ph.D. from UCLA. He was a postdoc at the University of Bristol (UK), and a Visiting Research Scientist at DuPont Central Research before joining the faculty at the University of Waterloo, Canada. He moved to the University of Durham (UK) in 1997 as Chair of Inorganic Chemistry and then to the University of Würzburg, Germany in 2012, also as Chair of Inorganic Chemistry. His diverse interests include conjugated optical materials, homogeneous catalysis, boron chemistry, crystal engineering, cell imaging, and bio-molecule sensing.